Designing of Plasmonic High Pass Wavelength Filter and Band Pass Filter

by

Md. Mahmudul Hasan (132460)
Mehedi Hasan (132454)
Dewan Saiham (132437)

A Thesis Submitted to the Academic Faculty in Partial Fulfillment of the Requirements for the Degree of

BACHELOR OF SCIENCE IN ELECTRICAL AND ELECTRONIC ENGINEERING

Department of Electrical and Electronic Engineering
Islamic University of Technology (IUT)
Gazipur, Bangladesh
13 November 2017

Designing of Plasmonic High Pass Wavelength Filter and Band Pass Filter

Approved by:

Dr. Rakibul Hasan Sagor

Thesis Supervisor,
Assistant Professor,
Department of Electrical and Electronic Engineering,
Islamic University of Technology (IUT),
Boardbazar, Gazipur-1704.

Date: ……

Table of Contents

List of Tables

List of Figures

List of Acronyms

ABC	Absorbing Boundary Condition
ADE	Auxiliary Differential Equation
DMD	Dielectric-Metal-Dielectric
FDTD	Finite Difference Time Domain
IMI	Insulator-Metal-Insulator
IR	Infra-Red
LD	Lorentz-Drude
MDM	Metal-Dielectric-Metal
MIM	Metal-Insulator-Metal
PLRC	Piecewise Linear Recursive Convolution
PML	Perfectly Matched Layer
SPP	Surface Plasmon Polariton
TE	Transverse Electric
TM	Transverse Magnetic

Acknowledgements

First and foremost, we offer gratitude to the Almighty Allah (SWT) for giving us the capability to do this work with good health.

We are grateful to our research supervisor, Dr. Rakibul Hasan Sagor, Assistant Professor, for the support and guidance throughout our research at Islamic University of Technology (IUT). He created a nice research environment for which we were able to explore many ideas without constraint. We have gained a wealth of knowledge and experience in science and engineering through his direction that is beyond value to our future endeavor. For all of his efforts as our true mentor, we express our heartfelt gratitude to him.

We would also like to express our gratitude to Mirza Fuad Adnan, Lecturer, for his inspiration and timely help that progressed our thesis work and made this such an educative journey. It is he, who filled up our lack of experience and knowledge with his great guidance and technical excellency. For his dedication to our research, we express our thanks to him.

We would like to thank all the faculty members of the department of EEE, IUT for their inspiration and help.

And last but not the least we are thankful to our family, friends and well-wishers for their support and inspiration. Without them it would never have been possible for us to make it this far.

Abstract

Plasmonic devices have become one of the most attractive research interest in present times due to its capability to overcome few of the shortcomings of electronic devices. One of the major advantage offered by the plasmonic devices is its ability to overcome diffraction limit that arises due to miniaturization of the devices. Among various types of plasmonic devices, plasmonic filters have attracted the eyes of researchers recently. Filters like high pass, low pass and band pass filters are noteworthy among the filter designs. Here, one nanoscale plasmonic high pass filter and one band pass filter designs are proposed using metal-insulator-metal (MIM) waveguide. The nanoscale plasmonic high pass filter consists of inward and outward grating profiles which are apodized by super Gaussian function and the band pass filter consists of ring resonator. The frequency dependent model of the metal is developed using Lorentz-Drude model which is solved numerically using finite-difference time-domain (FDTD) simulation in order to calculate the transmission efficiency of the filter. Changing various design parameters, the comparison of performance is also analyzed. Moreover, the proposed design is easier to fabricate since the simple geometrical shape is proposed.

Chapter 1

Introduction and Background

Plasmonic is becoming one of the major fields of research in recent times. Surface Plasmon Polaritons (SPPs) can localize the optical signals beyond the diffraction limit which enables SPPs to become such an important topic of research[1, 2]. SPPs provide opportunities to confine light on sub-wavelength scales along with low bending losses [3, 4]. Applications of SPPs cover the fields of bio sensing [5, 6], cloaking, integrated optics and much more [7].

Basic plasmonic structures include metal-insulator-metal (MIM) and insulator-metal-insulator (IMI) [8]. MIM structure is advantageous over IMI structure having higher confinement factor of light with an acceptable propagation length [8] and suitable for fabrication into optical devices.

In modern technologies, faster data rate of the data processing has become a major concern. To shorten the electron transit times less, the devices need to be miniaturized. The miniaturization resulted in a rapid increase of a tunneling current by 4th orders in the magnitude. Optical devices solve a lot of problems associated with traditional electronics. Photons travelling on optical fibers or thin film will be used in those optical processors making the system lighter and more compact [9, 10].

Modern communication system is mostly dependent on the optical fibers which offer high bandwidth and low loss than electronic interconnections. The same advantage can be availed if the optical technology is used in computer chips. Also, the optical chips will not require any insulation since photons do not interact with each other, making the system lighter. However, the diffraction limit of light restricts the application of conventional optics in making nanometer scale integrated circuits. According to the diffraction limit rule, light cannot propagate through aperture that is smaller than half of its wavelength.

Different devices like filters [11, 12], logic gates [13], biosensors [6] etc. are being designed recently using the sensitivity of different optical properties of MIM and IMI structures.

Plasmonic high pass wavelength or low pass frequency filters [11, 14, 15] and low pass wavelength or high pass frequency filters [16] are getting attentions of the researchers. Generally filters are designed using Fiber Bragg Grating [17, 18] and ring resonator [12, 19, 20]. But both of these can only be used to design band pass filters since they can only attenuate a certain range of frequency band. As a result, low pass or high pass filters cannot be designed [15].

Here a high pass wavelength plasmonic filter has been proposed using grating profiles which are apodized by super Gaussian function and the dependency of the cut-off wavelength on the different structural parameters have been analyzed. Moreover, a band pass filter is also designed using ring resonator.

1.1 Literature Review

Although plasmonic effects have been known for more than a century, the history of plasmon based applications began in the early 1970s, when Martin Fleischmann, a chemist at the University of Southampton, UK, and others began to study how light scatters from molecules stuck to a silver surface [21].

The plasmonic high pass filter are not been reported to be designed till 2011 [11]. So there is still a huge scope for researchers in this field. Here in this section, literature review of the published works on SPP propagation analysis through different structures with different geometries and most importantly filters are discussed.

The optical constants of noble metals (copper, gold and silver) are determined by Johnson et al. [22] in early 1980s. The modified Debye model parameters for gold which are applicable in the wavelength range of 550-950 nm are determined by Jin et al. [23]. Krug et al. [24] reported the gold parameters that are applicable in the

wavelength range of 700-1000 nm. A.D. Rakic et al.[25] reported the parameters for Nickel, Palladium, Titanium and 8 other metals using Lorentz-Drude and Brendel-Bormann Model. M.A. Ordal et al. [26] extracted the parameters for fourteen metals in the infrared and far-infrared range.

In optoelectronic devices, recombination, bend, splitter or grating play very important role for propagation of light. G. Veronis et al. [27] showed that bends and splitters can be designed over a wide frequency range without much loss by keeping centre layer thickness small compared to wavelength. H. Gao et al. [28] investigated the propagation and combination of SPP in Y-shaped channels. B. Wang et al. [29]analyzed two structures which consist of splitting and recombination.

Designing efficient nanoplasmonic couplers with different materials and structures can be a pioneering step in miniaturization of the integrated photonic devices. In the past years, several plasmonic couplers have been proposed by different researchers. G. Veronis et. al. [30] proposed a coupler with multi-section tapers. P. Ginzburg et al. [31] reported a $\lambda/4$ coupler to couple optical modes from a 0.5m to 50nm wide plasmonic waveguide. D. Pile et al. [32] presented an adiabatic and a non-adiabatic tapered plasmonic coupler. R. Washleh et al. [33] reported an analysis on nanoplasmonic air-slot coupler and its fabrication steps.

Yu Wang [34] proposed Surface-plasmon-wave-coupled tunable filter, which is the first plasmonic filter design known. Plamonic filters are recently designed using Fiber Bragg grating [17, 18], ring resonator[12, 19, 20]. For designing of plasmonic filters metal-insulator-metal (MIM) structure is very popular. Metal-insulator-metal (MIM) waveguide is considered to have unique advantages because of its strong field localization, simplicity, and being convenient for fabrication and integration into optical circuits [11]. First high pass filter design was proposed by Zhu et al. [11].

The implementation of grating in high pass plasmonic filter is yet to be proposed till this design. However, some properties of MIM grating structure like optical delay lines

are analyzed by Saeed khan et al. [35-37].The band pass filters are popularly designed using Fiber Bragg grating and ring resonator.

1.2 Thesis objective:

The main objective of the thesis is to design plasmonic filters. In this thesis high pass wavelength or low pass frequency filter and band pass filter are developed. The simulation output as transmission efficiency verifies the proposed MIM structures as high pass and band pass filters. More specifically, the objectives are

- To develop a plasmonic filter with high pass and band pass properties individually.
- To develop a simulation model based on the FDTD method that is capable of simulating the devices.
- To verify the possibility of fabrication of these structures into nanoscale devices.
- To explore different dimensions of nanoscale plasmonic devices and its fabrication.
- To summarize important conclusions from the obtained results and discuss the potential applications.

1.3 Overview surface plasmon polariton

There are 3 types of elementary excitations, namely
• Phonons
• Plasmons
• Excitons (bound electron-hole pair)

Polaritons:
Coupled state between an elementary excitation and a photon.

Plasmon polariton:
coupled state between a plasmon and a photon.

Phonon polariton:
coupled state between a phonon and a photon.

Surface plasmon polaritons:
Maxell´s theory shows that EM surface waves can propagate also along a metallic

surface with a broad spectrum of eigen frequencies

from ω = 0 up to ω = $\omega p/\sqrt{2}$

Surface plasmon polaritons are electromagnetic excitations propagating at the interface between a dielectric and a conductor, evanescently confined in the perpendicular direction [7]. These electromagnetic surface waves arise via the coupling of the electromagnetic fields to oscillations of the conductor's electron plasma.

The eigenmodes of an interface between a dielectric and a metal are surface plasmon polaritons (SPP) [38]. We refer to them as eigenmodes in the sense that they are solutions of Maxwell's equations that can be formulated in the absence of an incident field. On a flat interface between dielectric and metal half-spaces with dielectric constants ε_d and ε_m, respectively, SPPs are transverse magnetic (TM) plane waves propagating along the interface. Assuming the interface is normal to z and the SPPs propagate along the x direction, the SPP wave vector k_x is related to the optical frequency through the dispersion relation [21].

$$k_x = k_o\sqrt{\in_d \in_m /(\in_d + \in_m)} \tag{1.1}$$

where $ko = \omega/c$ is the free-space wave vector. We take ω to be real and allow kx to be complex, since our main interest is in stationary monochromatic SPP fields in a finite area [39].The details of SPP has been discussed in Chapter 2.

1.4 Thesis Organization

The research presented in this dissertation aims at application of plasmonics to design low pass or band pass filter using the optical properties of metal-dielectric-metal interface. So this thesis is organized in the following way-

- Chapter 1 introduces the background and motivation to work in plasmonic devices with literature review.
- In chapter 2, the basic theories of SPPs are explained with derivation using mathematical equations of its propagation and dispersion in single or double interface(MDM).
- Chapter 3 describes the modeling of metals with necessary derivation. Since SPPs are created due to the coupling of photon energy to the free electrons of

metal, modeling metals is one of the key steps for the simulation of SPP propagation.

- In chapter 4, the FDTD simulation model has been developed so that the simulation can be run in MATLAB®. The mathematical calculation is done and explained for the 1D and 2D simulations. The original formulations of Yee do not include the frequency dependent dispersion properties of materials. We have used the ADE based general algorithm for our simulation model which is discussed in Chapter 4. This chapter also discusses about the absorbing boundary condition.
- In chapter 5 modified Debey model, Lorentz model is discussed and also a developed simulation model is established.
- In chapter 6, the designing of plamonic high pass wavelength or low pass frequency filter is described in details with description of the structures and their performance with the help of MATLAB® simulation. Comparison of the performance of different structures are also discussed.
- In chapter 7, the designing of plasmonic band pass filter is described in details with structures and their performance analysis in MATLAB® simulation. Comparison of the performance of different structures are also discussed.
- Chapter 8 is about the future work and conclusion.

Chapter 2

SPP propagation Theory

2.1 Introduction

Surface plasmon polariton (SPP) is an electromagnetic excitation that propagates in a wave like fashion along the planar interface between a metal and a dielectric medium, often vacuum, and whose amplitude decays exponentially with increasing distance into each medium from the interface. Electromagnetic wave propagation is obtained from the solution of Maxwell's equations in each medium, and the associated boundary conditions. Maxwell's equations of macroscopic electromagnetism can be written as follows:

From Gauss's Law for the electric field

$$\nabla.D = \rho_{ext} \tag{2.1}$$

From Gauss's Law for the magnetic field

$$\nabla.B = 0 \tag{2.2}$$

From Faraday's Law

$$\nabla \times E = -\frac{\partial B}{\partial t} \tag{2.3}$$

From Ampere's Law

$$\nabla \times H = J_{ext} + \frac{\partial D}{\partial t} \tag{2.4}$$

Here,

E is the electric field vector in volt per meter

D is the electric flux density vector in coulombs per square meter

H is the magnetic field vector in amperes per meter

B is the magnetic flux density vector in webers per square meter

ext is the charge density

Jext is the current density

The four macroscopic fields can be also linked further via the polarization P and magnetization M by

$$D = \varepsilon_o E + P \tag{2.5}$$

$$H = \frac{1}{\mu_o} B - M \tag{2.6}$$

Now these equations can be simplified for linear, isotropic, nonmagnetic media as

$$D = \varepsilon_o \varepsilon_r E \tag{2.7}$$

$$B = \mu_o \mu_r H \tag{2.8}$$

where,

ε_0 is electric permittivity of vacuum in Farad per meter

$\mu_0$is the magnetic permeability of vacuum in Henry per meter

$\varepsilon_r$is the relative permittivity

$\mu_r$is the relative permeability

2.2 The EM or Electromagnetic Wave Equation

The EM wave equation which describes the field amplitude in time and space can be derived from Maxwell's equations. The wave equation can be derived by taking curl of Faraday's law

$$\nabla \times \nabla \times E = -\frac{\partial B}{\partial t} \tag{2.9}$$

or,

$$\nabla \times \nabla \times E = \nabla \times (-\mu \frac{\partial H}{\partial t}) \tag{2.10}$$

with the identities $\nabla \times \nabla \times E = \nabla(\nabla.E) - \nabla^2 E$ and $\nabla \times H = \varepsilon \frac{\partial E}{\partial t}$ we can simplify the above equation as

$$\nabla(\nabla.E) - \nabla^2 E = -\mu\varepsilon \frac{\partial^2 y}{\partial t^2} \tag{2.11}$$

From Gauss's law we can conclude that the divergence of E in a constant permittivity over space is zero. i,e $\nabla.E = 0$

Therefore, the final wave equation for electric field will be

$$\nabla^2 E - \mu\varepsilon \frac{\partial^2 E}{\partial t^2} = 0 \qquad (2.12)$$

Similarly, the wave equation for magnetic field can be derived as

$$\nabla^2 H - \mu\varepsilon \frac{\partial^2 H}{\partial t^2} = 0 \qquad (2.13)$$

So, the general form of wave equation can be written as

$$\nabla^2 U - \frac{1}{v_p^2}\left(\frac{\partial^2 H}{\partial t^2}\right) = 0 \qquad (2.14)$$

If the variation of the dielectric profile " is negligible over distance, then we can write

$$\nabla^2 E - \frac{\varepsilon}{C^2}\frac{\partial^2 E}{\partial t^2} = 0 \qquad (2.15)$$

where $C = \frac{1}{\sqrt{\mu_o \varepsilon_o}}$, velocity of light

The solution of wave equation is a harmonic function in time and space. Now if we assume this as a harmonic time dependence of the electric field,

$$E(r,t) = E(r)e^{-j\omega t} \qquad (2.16)$$

Therefore, we get the Helmholtz equation

$$\nabla^2 E + K_0^2 \varepsilon E = 0 \qquad (2.17)$$

where the vector of propagation $K_0 = \frac{\omega}{C}$ in free space.

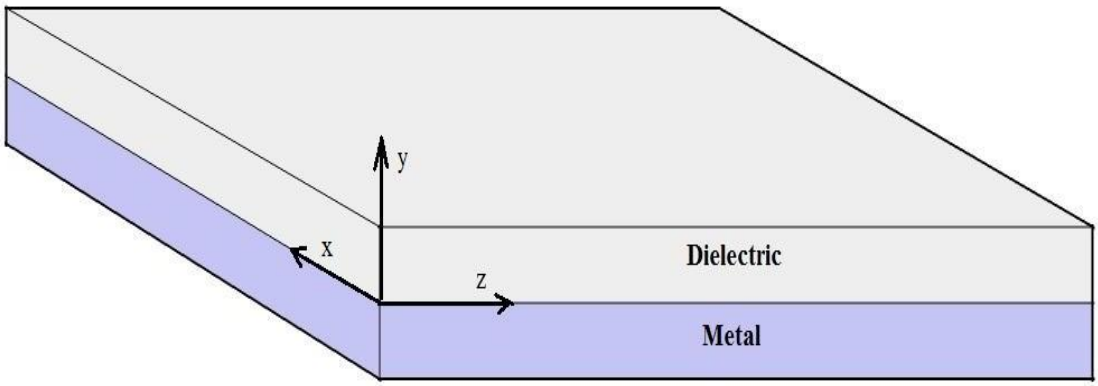

Fig. 2.1: Typical planar waveguide geometry. The waves propagate along the x-direction in a Cartesian coordinate system

For simplicity let us assume the propagation of wave is along the x-direction of the Cartesian co-ordinate system and no spatial variation in y-direction. So we can write

$$E(x,y,z) = E(z)e^{j\beta z} \qquad (2.18)$$

Where $\beta = K_x$ which is call the propagation constant

Now inserting the value of E the wave equation will be

$$\frac{\partial^2 E(z)}{\partial z^2} + (K_0^2 \varepsilon - \beta^2)E = 0 \tag{2.19}$$

Similarly, we can derive the equation for the magnetic field H. The field E and H can be decomposed in Cartesian co-ordinate system as

$$E = E_x \vec{a}_x + E_y \vec{a}_y + E_z \vec{a}_z \tag{2.20}$$

$$H = H_x \vec{a}_x + H_y \vec{a}_y + H_z \vec{a}_z \tag{2.21}$$

For Harmonic time dependence $\frac{\partial}{\partial t} = -j\omega$ and by solving the Ampere's law and Faraday's law, we get

$$\frac{\partial E_z}{\partial y} - \frac{\partial E_y}{\partial z} = j\omega\mu_0 H_x \tag{2.22}$$

$$\frac{\partial E_x}{\partial z} - \frac{\partial E_z}{\partial x} = j\omega\mu_0 H_y \tag{2.23}$$

$$\frac{\partial E_y}{\partial x} - \frac{\partial E_x}{\partial y} = j\omega\mu_0 H_z \tag{2.24}$$

$$\frac{\partial H_z}{\partial y} - \frac{\partial H_y}{\partial z} = j\omega\varepsilon_0 \varepsilon E_x \tag{2.25}$$

$$\frac{\partial H_x}{\partial z} - \frac{\partial H_z}{\partial x} = j\omega\varepsilon_0 \varepsilon E_y \tag{2.26}$$

$$\frac{\partial H_y}{\partial x} - \frac{\partial H_x}{\partial y} = j\omega\varepsilon_0 \varepsilon E_z \tag{2.27}$$

As the propagation is in x-direction in the form of $e^{j\beta x}$ which follows $\frac{\partial}{\partial x} = -j\beta$.

The homogeneity in y- direction make $\frac{\partial}{\partial y} = 0$. So the equation will be simplified as

$$-\frac{\partial E_y}{\partial z} = j\omega\mu_0 H_x \tag{2.28}$$

$$\frac{\partial E_x}{\partial z} - j\beta E_z = j\omega\mu_0 H_y \tag{2.29}$$

$$j\beta E_y = j\omega\mu_0 H_z \tag{2.30}$$

$$\frac{\partial H_y}{\partial z} = j\omega\varepsilon_0\varepsilon E_x \tag{2.31}$$

$$\frac{\partial H_x}{\partial z} - j\beta H_z = j\omega\varepsilon_0\varepsilon E_y \tag{2.32}$$

$$j\beta H_y = j\omega\varepsilon_0\varepsilon E_z \tag{2.33}$$

The solution of the above equation can be characterized by two sets of solution with the polarized characteristics which are, Transverse Magnetic (TM) modes and Transverse Electric (TE) modes. The equations belong to TM modes are

$$E_x = -j\frac{1}{\omega\varepsilon_0\varepsilon}\frac{\partial H_y}{\partial z} \tag{2.34}$$

$$E_z = -\beta\frac{1}{\omega\varepsilon_0\varepsilon}H_y \tag{2.35}$$

Therefore, the wave equation for TM Polarized wave will be

$$\frac{\partial^2 H_y}{\partial z^2} + (K_0^2\varepsilon - \beta^2)H_y = 0 \tag{2.36}$$

Similarly, the TE polarized equations will be

$$H_x = j\frac{1}{\omega\mu_0}\frac{\partial E_y}{\partial z} \tag{2.37}$$

$$H_y = \beta\frac{1}{\omega\mu_0}E_y \tag{2.38}$$

And the corresponding TE wave equation will be

$$\frac{\partial^2 E_y}{\partial z^2} + (K_0^2\varepsilon - \beta^2)E_y = 0 \tag{2.39}$$

2.3 SPP at Single Interface

The simplest configuration of SPP propagation is at single interface, that is in between dielectric, having the positive dielectric constant $\varepsilon 2$ and metal, having the negative dielectric constant $\varepsilon 1$. For metal the bulk Plasmon frequency will be ωp and the amplitude decays perpendicular to the z− direction.

For the TM solutions in both spaces: metal and dielectric will be for z > 0

$$H_z(\mathrm{z}) = \mathrm{A}_2 \mathrm{e}^{j\beta x} \mathrm{e}^{-k_2 z} \tag{2.40}$$

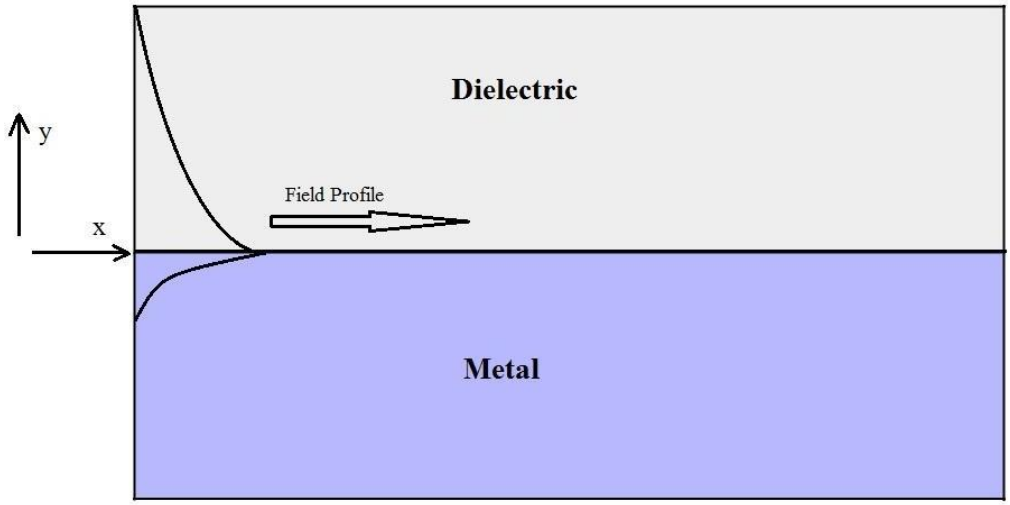

Fig. 2.2: SPP at the Single interface.

$$E_x(\mathrm{z}) = \mathrm{jA}_2 \frac{1}{\omega \varepsilon_0 \varepsilon_2} k_2 e^{j\beta x} e^{-k_2 z} \tag{2.41}$$

$$E_x(\mathrm{z}) = \mathrm{jA}_2 \frac{1}{\omega \varepsilon_0 \varepsilon_2} k_2 e^{j\beta x} e^{-k_2 z} \tag{2.42}$$

And for z < 0

$$H_y(\mathrm{z}) = \mathrm{A}_1 e^{j\beta x} e^{k_1 z} \tag{2.43}$$

$$E_x(\mathrm{z}) = -\mathrm{jA}_1 \frac{1}{\omega \varepsilon_0 \varepsilon_1} k_1 e^{j\beta x} e^{k_1 z} \tag{2.44}$$

$$E_x(\mathrm{z}) = -\mathrm{A}_1 \frac{\beta}{\omega \varepsilon_0 \varepsilon_1} e^{j\beta x} e^{-k_1 z} \tag{2.45}$$

The continuity of H_y and $\varepsilon_i E_z$ at the metal dielectric interface gives $A_1 = A_2$ and

$$\frac{k_2}{k_1} = -\frac{\varepsilon_2}{\varepsilon_1} \tag{2.46}$$

The surface wave exists at the metal dielectric interface with opposite sign of their real dielectric permittivities. So, we can write

$$k_1^2 \varepsilon = \beta^2 - k_0^2 \varepsilon_1 \tag{2.47}$$

$$k_2^2 \varepsilon = \beta^2 - k_0^2 \varepsilon_2 \tag{2.48}$$

The dispersion relation of SPPs propagation can be found as

$$\beta = k_0 \sqrt{\frac{\varepsilon_1 \varepsilon_2}{\varepsilon_1 + \varepsilon_2}} \tag{2.49}$$

The TE surface modes can be expressed as

$$E_y(\mathrm{z}) = \mathrm{A}_2 \, e^{j\beta x} e^{-k_2 z} \tag{2.50}$$

$$H_x(\mathrm{z}) = -j \, \mathrm{A}_2 \frac{\beta}{\omega \mu_0} k_2 e^{j\beta x} e^{-k_2 z} \tag{2.51}$$

$$H_z(\mathrm{z}) = \mathrm{A}_2 \frac{\beta}{\omega \mu_0} k_2 e^{j\beta x} e^{-k_2 z} \tag{2.52}$$

for z > 0, and

$$E_y(\mathrm{z}) = \mathrm{A}_1 \, e^{j\beta x} e^{-k_1 z} \tag{2.53}$$

$$H_x(\mathrm{z}) = j \, \mathrm{A}_1 \frac{\beta}{\omega \varepsilon_0 \varepsilon_1} k_1 e^{j\beta x} e^{k_1 z} \tag{2.54}$$

$$H_z(\mathrm{z}) = \mathrm{A}_1 \frac{\beta}{\omega \varepsilon_0 \varepsilon_1} k_2 e^{j\beta x} e^{k_1 z} \tag{2.55}$$

for z < 0. The continuity of E_y and H_x requires

$$A_1 (k_1 + k_2) = 0 \tag{2.56}$$

The surface requires that the real part of k_1 and k_2 should be greater than zero for confinement. This will be satisfied if A1 = A2 = 0. Therefore, no surface modes for the TE polarization. SPP only exist for TM mode polarization.

2.4 SPP at Double Interface

Two mostly used double interface configurations of SPP waveguides are: Metal-Dielectric-Metal(MDM) and Dielectric-Metal-Dielectric (DMD). In these cases, SPPs are formed on both interfaces. When the distance is shorter than decay distance, it forms coupled mode of SPP. This coupled mode of propagation can also be sub-divided into even and odd modes, as shown in the figure

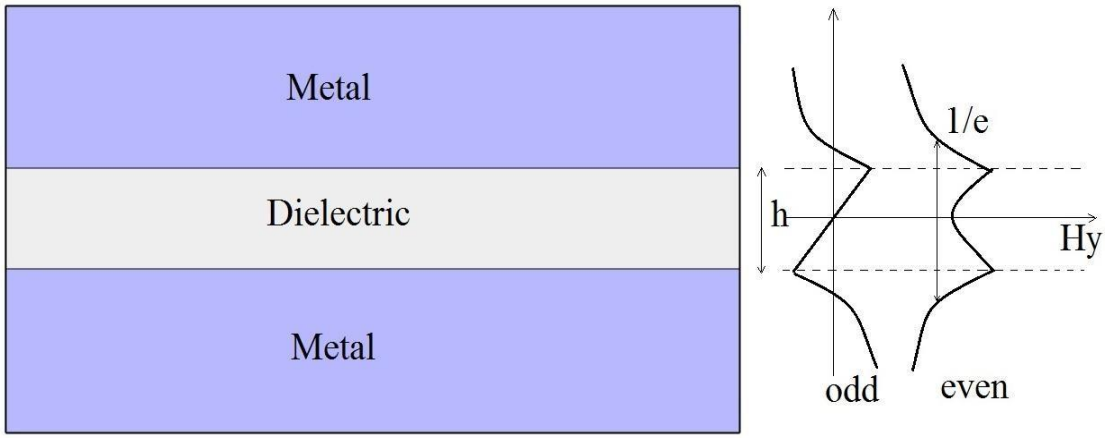

Fig. 2.3: SPP at the double interface

Chapter 3

Material Modeling Within Optical Range

3.1 Introduction

At low frequencies or for long wavelengths metals act as perfect conductors. Since it has zero field, they do not show any dispersive behavior. But at higher frequencies such as optical range metals behave as dispersive materials which means that there exists field inside metal. And for the frequencies higher than optical range metals act as dielectrics. Properties of SPPs depend highly on the material response to light. In this chapter we will be studying about the material supporting SPP, descriptions and derivations of different models for describing the behavior of metal in the presence of light.

Now in presence of an external oscillating electromagnetic field, three vectors can determine the behavior of any material. Such as: D (electrical flux density), E (electric field intensity) and P (polarization density). In frequency domain the corresponding equation will be

$$D(\omega) = \varepsilon(\omega)\,\mathrm{E}(\omega) \tag{3.1}$$

$$P(\omega) = \varepsilon_0 \chi(\omega)\,\mathrm{E}(\omega) \tag{3.2}$$

$$D(\omega) = \varepsilon_0\,\mathrm{E}(\omega) + P(\omega) \tag{3.3}$$

Combining these two equations we get

$$D(\omega) = \varepsilon_0\,\mathrm{E}(\omega)(1+\chi(\omega)) \tag{3.4}$$

Where χ is the electric susceptibility which measures how easily it is polarized in response to an applied electric field, and it is a dimensionless quantity.

Finally, the relation between the permittivity and susceptibility is

$$\varepsilon(\omega) = \varepsilon_0(1+\chi(\omega)) \tag{3.5}$$

So the relative permittivity will be

$$\varepsilon_r(\omega) = 1 + \chi(\omega) \tag{3.6}$$

For linear isotropic materials such as glass this above values become simple. But for a dispersive material, the frequency dependent permittivity and susceptibility should be modeled perfectly for getting the perfect response of the material for certain electromagnetic excitation. Some widely used material models are Drude model, Lorentz model, Debye model and Lorentz-Drude model.

3.2 Different Material Models

3.2.1 The Drude Model

The Drude model of electrical conduction was first developed by Paul Drude. In his model he described the metal as a volume filled with stationary positive ions, immersed in a gas of electrons following the kinetic theory of gases. These electrons are free to move inside the metal without any interaction with each other. The electrons in a metal are subjected to two forces, such as

1. Driving force Fd
2. Damping force Fg

The driving force and the damping force can be expressed as

$$F_d = qE = -eE \tag{3.7}$$

$$F_g = -\Gamma \nu \tag{3.8}$$

As the two forces are opposite to each other, the resultant force will be

$$F = F_d - F_g \tag{3.9}$$

From Newton's first law of motion we can write

$$mr'' = -eE + \Gamma r' \tag{3.10}$$

where,

m is the mass of an electron

Γ is the damping constant in Newton second per meter

r is the displacement in meter.

v is the velocity of the electron.

q is the electrons charge.

The prime indicates differentiation order with respect to time

For time harmonic electric field and time harmonic displacement the equation will be

$$E(t) = \mathrm{E}_0\, e^{-j\omega t} \Leftrightarrow E(\omega) \tag{3.11}$$

$$\mathrm{r}(t) = R_0 e^{-j\omega t} \Leftrightarrow R(\omega) \tag{3.12}$$

From equation 3.10 the frequency domain form will be

$$\mathrm{mR}''(\omega) - \Gamma\, \mathrm{mR}'(\omega) + eE(\omega) = 0 \tag{3.13}$$

The derivatives of frequency domain will give

$$\mathrm{m}\,\omega^2\, \mathrm{R}''(\omega) - j\omega\Gamma\, \mathrm{mR}'(\omega) + eE(\omega) = 0 \tag{3.14}$$

Simplifying the above equation, the displacement R will give

$$R(\omega) = \frac{-e}{m(j\Gamma\omega - \omega^2)} E(\omega) \tag{3.15}$$

The polarization for *n* number of electrons will be

$$P(\omega) = -neR(\omega) \tag{3.16}$$

Or,

$$P(\omega) = \frac{e^2 n}{m(j\Gamma\omega - \omega^2)} E(\omega) \tag{3.17}$$

An expression for the susceptibility can also be obtained from the above equation and that will be

$$\frac{P(\omega)}{\varepsilon_0 E(\omega)} = \frac{e^2 n}{\varepsilon_0 m(j\Gamma\omega - \omega^2)} = \chi(\omega) \tag{3.18}$$

Now substituting this value in equation 3.6 we get

$$\varepsilon_r(\omega) = 1 + \frac{e^2 n}{\varepsilon_0 m(j\Gamma\omega - \omega^2)} \tag{3.19}$$

if we consider ωp as the plasma frequency that will provide

$$\omega_p^2 = \frac{e^2 n}{\varepsilon_0 m} \tag{3.20}$$

So, the frequency dependent flux density will be

$$D(\omega) = \varepsilon_0 (1 + \frac{\omega_p^2}{(j\Gamma\omega - \omega^2)}) E(\omega) \tag{3.21}$$

For low frequency, the term $\Gamma\omega \ll 1$ therefore, the dispersive relation can be reduced to

$$D(\omega) = \varepsilon_0 (1 - \frac{\omega_p^2}{\omega^2}) E(\omega) \tag{3.22}$$

3.2.2 The Lorentz Model

The Lorentz model gives a simpler picture of the atom. The model is a very useful tool to visualize atom-field interaction. In this model, Lorentz modeled an atom as a mass (nucleus) connected to another smaller mass (electron). However, electrons in the Lorentz model do not move freely inside the metal instead, they are bound to atoms. So, there is a restoring force acting between them which can be denoted by Fr

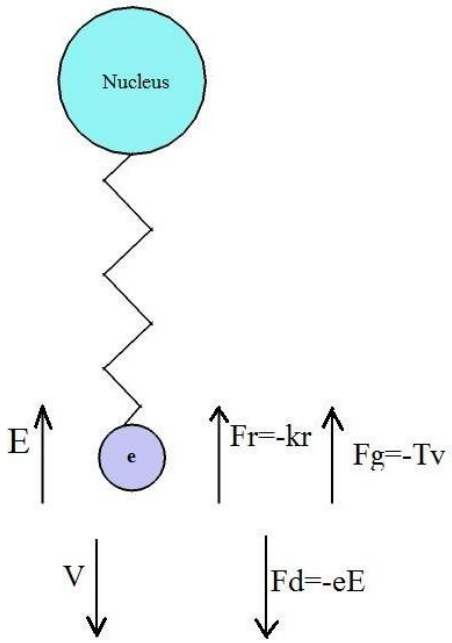

Fig. 3.1: Lorentz model

The restoring force can be written as

$$F_r = -kr \tag{3.23}$$

where k is the spring constant in Newtons per meter.

Similarly, from the law of motion we can say that

$$mr'' + \Gamma mr'(\omega) + \mathrm{mkr} + \mathrm{eE} = 0 \tag{3.24}$$

In frequency domain the above equation will be

$$\mathrm{R}(\omega)(\mathrm{m}\omega_0^2 + j\omega\Gamma m - m\omega^2 - eE(\omega) = 0 \tag{3.25}$$

Considering the natural frequency $\omega_0 = \sqrt{\frac{k}{m}}$ we get

$$\mathrm{R}(\omega) = \frac{-e}{\mathrm{m}(\omega_0^2 + j\omega\Gamma - \omega^2)}\mathrm{E}(\omega) \tag{3.26}$$

Therefore, the susceptibility can be found as

$$\frac{P(\omega)}{\varepsilon_0 E(\omega)} = \frac{e^2 n}{\varepsilon_0 m(\omega_0^2 + j\omega\Gamma - \omega^2)} = \chi(\omega) \tag{3.27}$$

So, from the equation 3.4 the expression for D can be expressed in frequency domain as

$$D(\omega) = \varepsilon_0(1+\frac{\omega_p^2}{\omega_0^2 + j\omega\Gamma - \omega^2})E(\omega) \tag{3.28}$$

3.2.3 The Lorentz-Drude Model

In the Lorentz-Drude (LD) model, which is the most general form when an EM field is applied to a metal, the electrons of two types oscillate inside the metal, and they contribute to the permittivity. The free electrons contribute a permittivity of the Drude model, and the bound electrons contribute a permittivity of the Lorentz model. The permittivity in the LD model is given by

$$\varepsilon = \varepsilon_{free} + \varepsilon_{bound} \tag{3.29}$$

Where

$$\varepsilon_{free} = 1+\frac{\omega_p}{(\mathrm{j}\Gamma\omega - \omega^2)} \tag{3.30}$$

$$\varepsilon_{bound} = \frac{\omega_p}{\omega_0 + \mathrm{j}\Gamma\omega - \omega^2} \tag{3.31}$$

Therefore, combining both the model together the electric field density D in frequency domain will be

$$D(\omega) = \varepsilon_0(1+\frac{\omega_p}{\mathrm{j}\Gamma\omega - \omega^2} + \frac{\omega_p}{\omega_0 + \mathrm{j}\Gamma\omega - \omega^2})E(\omega) \tag{3.32}$$

The above relation is known as the Lorentz-Drude model.

3.2.4 The Debye Model

The Debye model was first developed by Peter Debye in the year 1912. According to the Debye model materials are made of electric dipoles, so that, when an electric field is applied, these dipoles follow the behavior of the applied field with some relaxation time. If the electric field is oscillating at a slow frequency, then the polarization will be

strong. On the other hand, a fast oscillating field means low polarization. From another point of view, materials with long relaxation times have low polarization or no polarization at all, and materials with short relaxation times have strong polarization.

Metals are known to have very short relaxation times. Thus, polarization in metals is strong. If a DC electric field is applied to a dielectric, the polarization takes some time to follow the electric field. At steady state, it will be

$$P(\mathrm{t}) = \mathrm{P}_{\infty}(1-\mathrm{e}^{-t/\tau}) \tag{3.33}$$

where P (t) is the instantaneous polarization

P∞ is the polarization in the steady state is the time constant.

The derivative of the above equation will be

$$\frac{dP(\mathrm{t})}{dt} = \frac{1}{\tau}\mathrm{P}_{\infty}\mathrm{e}^{-t/\tau} \tag{3.34}$$

Now combining both the equations we get

$$P(t) = \mathrm{P}_{\infty} - \tau\frac{dP(\mathrm{t})}{dt} \tag{3.35}$$

As $\mathrm{P}_{\infty} = \varepsilon_0(\varepsilon - 1)$ so the equation will be reduced to

$$\mathrm{P}(\mathrm{t}) = \varepsilon_0(\varepsilon - 1)E(t) - \tau\frac{dP(\mathrm{t})}{dt} \tag{3.36}$$

or,

$$\varepsilon_0(\varepsilon - 1)E(t) = \mathrm{P}(\mathrm{t}) + \tau\frac{dP(\mathrm{t})}{dt} \tag{3.37}$$

In frequency domain the equation will be

$$\varepsilon_0(\varepsilon - 1)E(\omega) = \mathrm{P}(\varepsilon) + \mathrm{j}\omega\tau P(\omega) \tag{3.38}$$

or,

$$P(\omega) = \frac{\varepsilon_0(\varepsilon - 1)}{1 + \mathrm{j}\omega\tau}E(\omega) \tag{3.39}$$

The susceptibility can be expressed as

$$\frac{\varepsilon - 1}{1 + \mathrm{j}\omega\tau} = \frac{P(\omega)}{\varepsilon_0 E(\omega)} = \chi(\omega) \tag{3.40}$$

The relative permittivity will be

$$\varepsilon_0(\omega) = \frac{\varepsilon - 1}{1 + \mathrm{j}\omega\tau} + 1 = 1 + \chi(\omega) \tag{3.41}$$

For the permittivity function to fit in the range from 0 frequency to infinity frequency, the boundary conditions are $\varepsilon_r(0) = \varepsilon_s(0)$ and $\varepsilon_r(\infty) = \varepsilon_\infty(0)$

So,

$$\varepsilon(\omega) = \varepsilon_\infty + \frac{(\varepsilon_s - \varepsilon_\infty)}{1 + \mathrm{j}\omega\tau} \tag{3.42}$$

To take into account the material losses that SPPs encounter, another term is added with the permittivity of metal. So, the above equation can be expanded to

$$\varepsilon(\omega) = \varepsilon_\infty + \frac{(\varepsilon_s - \varepsilon_\infty)}{1 + \mathrm{j}\omega\tau} - j\frac{\sigma}{\omega\varepsilon_0} \tag{3.43}$$

In real and imaginary term, the Debye model is

$$\varepsilon_r(\omega) = \varepsilon'(\omega) - \mathrm{j}\varepsilon''(\omega) \tag{3.44}$$

where-

$$\varepsilon'(\omega) = \varepsilon_\infty + \frac{(\varepsilon_s - \varepsilon_\infty)\omega\tau}{1 + \mathrm{j}\omega^2\tau^2} \tag{3.45}$$

$$\varepsilon''(\omega) = \varepsilon_\infty + \frac{(\varepsilon_s - \varepsilon_\infty)\omega\tau}{1 + \mathrm{j}\omega^2\tau^2} + \frac{\sigma}{\omega\varepsilon_0} \tag{3.46}$$

3.3 Material Dispersion

Dispersion can be defined as the variation of the propagating waves wavelength with frequency. It is also sometimes defined as the variation of propagating waves wave number $k = \frac{2\pi}{\lambda}$ with angular frequency $\omega = 2\pi f$. So, the one dimensional wave equation will be

$$\frac{\partial^2 u}{\partial t^2} = v^2 \frac{\partial^2 u}{\partial x^2} \tag{3.47}$$

where,

$$v^2 = \frac{1}{\varepsilon\mu}$$

The solution of the above wave equation can be written in phasor form as

$$u(x,t) = \mathrm{e}^{j(\omega t - kx)} \tag{3.48}$$

Now putting this value in the wave equation, we get

$$(j\omega)^2 \mathrm{e}^{j(\omega t - kx)} = v^2(-jk)^2 \mathrm{e}^{j(\omega t - kx)} \tag{3.49}$$

Finally, from this equation we get

$$k = \pm\frac{\omega}{v} \tag{3.50}$$

The + sign is for -x directed wave propagation and - sign is for +x directed wave propagation. The magnetic flux density and electric flux density for dispersive medium are-

$$D(\omega) = \varepsilon(\omega)E \tag{3.51}$$

$$B(\omega) = \mu(\omega)H \tag{3.52}$$

Here both $\varepsilon(\omega)$ and $\mu(\omega)$ are frequency dependent functions.

Chapter 4

Overview of Finite-Difference Time-Domain Method

4.1 The Yee Algorithm

The algorithm used in FDTD simulations is known as the Yee algorithm. The original proposal was intended for homogeneous, isotropic and lossless media based on discretizing the volume into cells in Cartesian coordinates. The Yee algorithm solves for both electric and magnetic fields using the coupled Maxwell's time-dependent curl equations, rather than solving for the electric field alone (or the magnetic field alone) with a wave equation.

The method begins with two of Maxwell's equations:

$$D\frac{\partial \vec{H}}{\partial t} = -\frac{1}{\mu}\nabla \times \vec{E} \tag{4.1}$$

$$D\frac{\partial \vec{E}}{\partial t} = -\frac{1}{\varepsilon}\nabla \times \vec{H} \tag{4.2}$$

The electric and magnetic fields are three dimensional vectors. Each equation can be converted into three coupled scalars first order differential equations. The derivatives are both in space and time. The curl operations of equations 4.1 and equation 4.2 yields the following six equations in Cartesian coordinates

$$\frac{\partial E_z}{\partial y} - \frac{\partial E_y}{\partial z} = \mu\frac{\partial H_x}{\partial t} \tag{4.3}$$

$$\frac{\partial E_x}{\partial z} - \frac{\partial E_z}{\partial x} = \mu\frac{\partial H_y}{\partial t} \tag{4.4}$$

$$\frac{\partial E_y}{\partial x} - \frac{\partial E_x}{\partial y} = \mu\frac{\partial H_z}{\partial t} \tag{4.5}$$

$$\frac{\partial H_z}{\partial y} - \frac{\partial H_y}{\partial z} = \varepsilon\frac{\partial E_x}{\partial t} \tag{4.6}$$

$$\frac{\partial H_x}{\partial z} - \frac{\partial H_z}{\partial x} = \varepsilon\frac{\partial E_y}{\partial t} \tag{4.7}$$

$$\frac{\partial H_y}{\partial x} - \frac{\partial H_x}{\partial y} = \varepsilon \frac{\partial E_z}{\partial t} \tag{4.8}$$

Then the scalar differential equations are converted into difference equations. In order to do that, discretization is required for both space and time. For space discretization, Yee visualized the field components arranged within a unit cell (voxel). The electric field components are stored on the corresponding cell edges, while the magnetic field components are stored on the corresponding face centers. The fields are located in a way where each E component is surrounded by four

H components and vice versa, which leads to a spatially coupled system of field circulations corresponding to the law of Faraday and Ampere. The figure 4.1 shows the Yee's spatial grid.

Considering a two dimensional TM (Transverse Magnetic) polarized field case,

$$\frac{\partial E_x}{\partial t} = \frac{1}{\varepsilon} \frac{\partial H_z}{\partial y} \tag{4.9}$$

$$\frac{\partial E_y}{\partial t} = \frac{1}{\varepsilon} \frac{\partial H_z}{\partial x} \tag{4.10}$$

$$\frac{\partial H_z}{\partial x} = \frac{1}{\mu} \left(\frac{\partial E_x}{\partial y} - \frac{\partial E_y}{\partial x} \right) \tag{4.11}$$

Central difference approximation is applied in each of the equations 4.9, 4.10 and 4.11 which finally conclude in a spatial scalar difference equations in 4.12, 4.13 and 4.14.

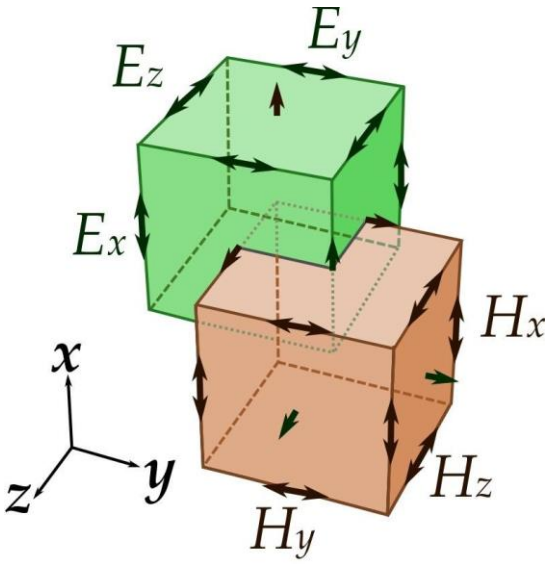

Fig. 4.1: Yee's spatial grid.

$$\frac{\partial E_x}{\partial t} = \frac{1}{\varepsilon}\frac{H_z(i,j) - H_z(i,j-1)}{\Delta y} \tag{4.12}$$

$$\frac{\partial E_y}{\partial t} = \frac{1}{\varepsilon}\frac{H_z(i,j) - H_z(i-1,j)}{\Delta x} \tag{4.13}$$

$$\frac{\partial H_z}{\partial t} = \frac{1}{\mu}\left(\frac{E_x(i,j+1) - E_x(i,j)}{\Delta y} - \frac{E_y(i+1,j) - E_y(i-1,j)}{\Delta x}\right) \tag{4.12}$$

In order to consider the time derivatives, the time axis is to be considered as shown in the figure. The Electric and Magnetic field are mapped half a step apart along the time axis. Again applying the central difference approximation the equations 4.12, 4.13 and 4.14 become:

$$\frac{E_x^{n+1}(i,j+\frac{1}{2}) - E_x^n(i+\frac{1}{2},j)}{\Delta t} = \frac{1}{\varepsilon}\frac{H_z^{n+\frac{1}{2}}(i+\frac{1}{2},j) - H_z^{n+\frac{1}{2}}(i+\frac{1}{2},j-\frac{1}{2})}{\Delta y} \tag{4.12i}$$

$$\frac{E_y^{n+1}(i,j+\frac{1}{2}) - E_y^n(i,j+\frac{1}{2})}{\Delta t} = \frac{1}{\varepsilon}\frac{H_z^{n+\frac{1}{2}}(i+\frac{1}{2},j+\frac{1}{2}) - H_z^{n+\frac{1}{2}}(i-\frac{1}{2},j+\frac{1}{2})}{\Delta y} \tag{4.13i}$$

$$\frac{H_z^{n+\frac{1}{2}}(i+\frac{1}{2},j+\frac{1}{2}) - H_z^{n-\frac{1}{2}}(i+\frac{1}{2},j+\frac{1}{2})}{\Delta t} = -\frac{1}{\mu}\left(\frac{E_x^{n+1}(i+\frac{1}{2},j+1) - E_x^n(i+\frac{1}{2},j)}{\Delta y} - \frac{E_y^n(i+1,j+\frac{1}{2}) - E_y^n(i,j+\frac{1}{2})}{\Delta x}\right) \tag{4.14i}$$

Each field component depends on the field of previous time step itself and the surrounding component in Yee's algorithm.

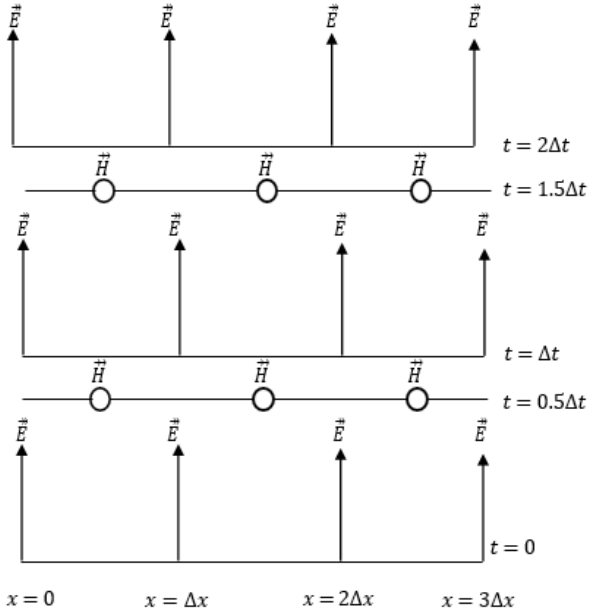

Fig. 4.2: The temporal scheme of FDTD method.

Numerical stability of the Yee algorithm is required to be ensured. In an unstable algorithm the computed magnitude of electric and magnetic field components will gradually increase without limit with the progression of simulation. To guarantee numerical stability, the EM field's propagation should not be faster than the al-lowed limit which is imposed by the phase velocity within the material. This is done by limiting time step Δt using the Courant-Friedrichs-Lewy criterion for the general Yee FDTD grid as follows:

$$\Delta t \leq \left\{ \frac{1}{v_p \sqrt{\frac{1}{(\Delta x)^2} + \frac{1}{(\Delta y)^2} + \frac{1}{(\Delta z)^2}}} \right\} \tag{4.15}$$

where Δx, Δy and Δz indicates the spatial Cartesian grid increments.

4.2 Absorbing Boundary Condition (ABC)

In FDTD method, a space of theoretically infinite extent with a finite computational cell is simulated due to limited computer resources. The boundary is said to be ideally absorbing, without any non-physical reflection back to the region. To accomplish this, a number of boundary conditions such as Berenger's perfectly matched layer (PML), have been proposed. An artificial layer surrounds the computational domain so that most of the outgoing waves are absorbed. The electromagnetic fields are made to attenuate rapidly until they become equal to zero, so that they do not produce any reflections.

4.3 Material Dispersion in FDTD

The material is said to be dispersive when the permittivity and permeability of a material are functions of frequency. In reality the assumption of constant relative permittivity is not absolutely correct. Because by doing so, instantaneous polarization of charge within a material is being assumed. In order to exploit the realistic wave propagation, dispersive FDTD techniques become necessary. The existing FDTD based algorithms for the analysis of material dispersion can be categorized into three types:

1) the auxiliary differential equation (ADE),
2) the Z-transform methods, and

3) methods base on discrete convolution of the dispersion relation or the recursive convolution (RC) method [40].

We will highlight on the ADE dispersive FDTD method as we have applied in material modeling. The other methods will also be briefly discussed.

4.3.1 The Auxiliary Differential Equation(ADE)

Taflove introduced the auxiliary differential equation to the FDTD modeling in order to integrate the dispersion relation into the model. The dispersion relation is converted from frequency domain to time domain through Fourier transform in the basic step of the procedure. The Fourier transform results in a relationship between the new E field value and the previous E and D values, which can be added to the algorithm to update the E fields. The new algorithm with ADE becomes

$$\frac{\partial}{\partial t} H_z = -\frac{1}{\mu}\left(\frac{\partial E_x}{\partial y} - \frac{\partial E_y}{\partial x}\right) \tag{4.16}$$

$$\frac{\partial}{\partial t} D_x = \frac{\partial H_z}{\partial y} \tag{4.17}$$

In order to get the function relating D to E in a dispersive medium, we start with

$$D(\omega) = \varepsilon_0 \frac{\sigma}{j\omega} E(\omega) \tag{4.18}$$

Multiplying by $j\omega$

$$j\omega D(\omega) = \varepsilon_0 \sigma E(\omega) \tag{4.19}$$

Applying the Fourier transform in equation 4.19

$$\frac{d}{dt} D(\mathrm{t}) = \varepsilon_0 \sigma E(\mathrm{t}) \tag{4.20}$$

Discretizing equation 4.20 equation using forward difference method

$$\frac{D^n - D^{n-1}}{\Delta t} = \varepsilon_0 \sigma E(\mathrm{t}) \tag{4.21}$$

Finally solving for *E*, we find the update equation

$$E^n = \frac{D^n - D^{n-1}}{\varepsilon_0 \sigma \Delta t} \tag{4.22}$$

4.3.2 The Z-transform Methods

The Z-transform is a faster method compared to ADE method. Sullivan used the Z-transform method for the first time in order to introduce the dispersion relation into the FDTD algorithm.

The Z-transform of the equation

$$D(\omega) = \varepsilon(\omega)\,\mathrm{E}(\omega) \tag{4.23}$$

is-

$$\mathrm{D(z)} = \varepsilon(\mathrm{z})\Delta\,\mathrm{tE(z)} \tag{4.24}$$

where ε(z) is the z-transform of $\varepsilon(\omega)$ and is the sampling period. As already done in ODE, let us consider the material dispersion as $\frac{\sigma}{j\omega}$, the relation between D and E is given by

$$D(\omega) = \frac{\sigma\varepsilon_0}{1-z^{-1}}\Delta\,\mathrm{tE(z)} \tag{4.25}$$

Multiplying by $(1-z^{-1})$, we find

$$D(\mathrm{z})(1-z^{-1}) = \sigma\varepsilon_0\,\mathrm{E(z)} \tag{4.26}$$

or,

$$D(\mathrm{z}) - z^{-1}D(\mathrm{z}) = \sigma\varepsilon_0\,\mathrm{E(z)} \tag{4.27}$$

Performing inverse z-transform

$$\mathrm{D}^n - \mathrm{D}^{n-1} = \sigma\varepsilon_0\Delta\,\mathrm{tE}^n \tag{4.28}$$

Finally, for solving E from equation 4.28, we find

$$\mathrm{E}^n = \frac{\mathrm{D}^n - \mathrm{D}^{n-1}}{\sigma\varepsilon_0\Delta\,\mathrm{t}} \tag{4.29}$$

Which is same as the final update equation derived by ADE method.

4.3.3 Piecewise Linear Recursive Convolution Method

Luebbers et al. formulated the first frequency dispersive FDTD algorithm using the recursive convolution (RC) scheme. Later it became piecewise linear recursive convolution(PLRC) method [41]. Initially developed for Debye media [40], the approach was later extended for the study of wave propagation in a Drude material [42], N-th order dispersive media [43], an anisotropic magneto-active plasma [44], ferrite material [44] and the bi-isotropic/chiral media [45-47].

The RC approach, typically being faster and having required fewer computer memory resources than other approaches, is usually less accurate. But in case of multiple pole mediums, it is easier to follow the RC approach.

In the initial derivation of PLRC method for a linear dispersive medium, the relation between electric flux density and electric field intensity is expressed as:

$$D(\mathrm{t}) = \varepsilon_\infty \varepsilon_0 E(t) + \varepsilon_0 \int_0^t E(t-\tau)\chi(\tau)\,\mathrm{d}\tau \tag{4.30}$$

which can be discretized as:

$$D^n = \varepsilon_\infty \varepsilon_0 E^n + \varepsilon_0 \int_0^{n\Delta t} E(n\Delta t-\tau)\chi(\tau)\,\mathrm{d}\tau \tag{4.31}$$

The PRC method is further preceded from this basing discrete equation.

4.3.4 The General Algorithm

The derivation of equations for multi-pole dispersion relation is more difficult compared to the single pole-pair dispersion relation. For example, for six-pole Lorentz-Drude dispersion the required derivation process is lengthy. Additionally, the memory required for computation is also vast. There are various methods proposed by researchers regarding this topic such as Taflove's matrix inversion method, Multi-term dispersion by Okoniewski, etc. However, Alsunaidi and Al-Jabr proposed a general algorithm technique which solves various problems regarding previous methods. The major advantage of this technique is that it requires only one algorithm for any dispersion relation. The dispersive relation has the general form as

$$D(\omega) = \varepsilon(\omega) + \mathrm{E}(\omega) \tag{4.32}$$

which can be expressed in terms of summation of poles

$$D(\omega) = \varepsilon_\infty \varepsilon_0\, \mathrm{E}(\omega) + \sum\nolimits_i^N P_i(\omega) \tag{4.33}$$

where N is the number of poles. Applying Fourier transform, this equation becomes

$$D^{n+1} = \varepsilon_\infty \varepsilon_0 E^{n+1} + \sum_i^N P_i^{n+1} \tag{4.34}$$

or,
$$E^{n+1} = \frac{D^{n+1} - \sum_i^N P_i^{n+1}}{\varepsilon_\infty \varepsilon_0} \tag{4.35}$$

This term Pi can be any form of dispersion relation such as the Debye, the Drude or just the conductivity term. This the final solved equation for E.

Chapter 5

Parameter Extraction of Optical Materials

The Modified Debye Model (MDM) parameters for silver metal is presented. A nonlinear optimization algorithm has been developed in order to extract the parameters for the metals. The extracted parameters have been used to determine the complex relative permittivity of the metals in optical and near-IR region of electromagnetic spectrum. The obtained results have been compared with the experimental values and an excellent agreement has been found.

5.1 Material Models

5.1.1 Modified Debye Model

5.1.1.1 Metals

The complex relative permittivity function of the modified Debye model is de-scribed by the following equation

$$\varepsilon_r(\omega) = \varepsilon_\infty + \frac{(\varepsilon_s - \varepsilon_\infty)}{1 + j\omega\tau} - j\frac{\sigma}{\omega\varepsilon_0} \tag{5.1}$$

where, ε_∞ is the infinite frequency relative permittivity, ε_s is the zero frequency, relative permittivity, ω is the angular frequency, σ is the conductivity and τ is the relaxation time.

If the model is represented in terms of its real and imaginary parts, then,

$$\varepsilon_r(\omega) = \varepsilon'(\omega) - \mathrm{j}\,\varepsilon''(\omega) \tag{5.2}$$

where, the real part of the complex relative permittivity is,

$$\varepsilon'(\omega) = \varepsilon_\infty + \frac{(\varepsilon_s - \varepsilon_\infty)}{1 + (\omega\tau)^2}$$

and the imaginary part of the complex relative permittivity is,

$$\varepsilon''(\omega) = \frac{(\varepsilon_s - \varepsilon_\infty)}{1 + (\omega\tau)^2} + \frac{\sigma}{\omega\varepsilon_0}$$

From equation 5.1, we can see that the modified Debye model can be described by four parameters which are ε_s, ε_∞, σ and τ. However, a relationship can be derived among these parameters by comparing equation 5.1 with the Drude model equation as,

$$\sigma = \frac{\varepsilon_0(\varepsilon_s - \varepsilon_\infty)}{\tau} \tag{5.3}$$

Now we actually have three parameters that need to be extracted and the other can be obtained from equation 5.3.

5.1.1.2 Dielectric Materials

The frequency dependent permittivity function of Modified Debye Model is given by

$$\varepsilon_r(\omega) = \varepsilon_\infty + \frac{(\varepsilon_s - \varepsilon_\infty)}{1 + j\omega\tau} \tag{5.4}$$

where, ε_∞ is the infinite frequency relative permittivity, ε_s is the zero frequency, relative permittivity, ω is the angular frequency and τ is the relaxation time.

From equation 5.4 we can see that modified Debye model for dielectric material can be described by three parameters which are ε_∞, ε_s and τ. These three parameters need to be optimized in order to model dielectric materials using MDM.

5.1.2 Lorentz Model

The frequency dependent complex permittivity function for single pole-pair Lorentz model is given by

$$\varepsilon_r(\omega) = \varepsilon_\infty + \frac{\omega_0^2(\varepsilon_s - \varepsilon_\infty)}{\omega_0^2 + j2\delta\omega - \omega^2} \tag{5.5}$$

where, ε_∞ is the infinite frequency relative permittivity, ε_s is the zero frequency, relative permittivity, ω_0 is the frequency of the pole pair and δ is the damping frequency.

From equation 5.5, it can be observed that single pole-pair Lorentz model can be described by four parameters which are $\varepsilon\infty$, εs, $\omega 0$ and δ. These four parameters are independent and need to be extracted.

5.1.3 Developing the Simulation Model

The simulation model we have developed is based on the FDTD method. We have utilized the general auxiliary differential equation (ADE) based FDTD approach in order to incorporate the frequency dependent dispersion property of the constituent materials. This algorithm is useful for the simulation of materials with different dispersive properties. The perfectly matched layer has been integrated at all the boundaries in order to prevent back reflections.

Considering the material dispersion, the frequency-dependent electric flux density can be given by-

$$D(\omega) = \in_0 \in_\infty E(\omega) + P(\omega) \tag{5.6}$$

The general Lorentz model for polarization (ω) is given by-

$$P(\omega) = \frac{a}{b + jc\omega - d\omega^2} E(\omega) \tag{5.7}$$

By inverse Fourier transform, it can be written in time domain as-

$$\mathrm{bP(t)} + c\,\mathrm{P}^{'}(\mathrm{t}) + d\,\mathrm{P}^{''}(\mathrm{t}) = \mathrm{aE(t)} \tag{5.8}$$

Now, turning to FDTD scheme, above equation can be presented as-

$$\mathrm{P}^{n+1} C_1 = C_1 \mathrm{P}^n + C_2 \mathrm{P}^{n-1} + C_3 E^n \tag{5.9}$$

Where, $C_1 = \frac{4d - 2b\Delta t^2}{2d + c\Delta t}$, $C_2 = \frac{-2d - c\Delta t}{2d + c\Delta t}$, $C_3 = \frac{2a\Delta t^2}{2d + c\Delta t}$

The values of $C1$, $C2$, $C3$ depends on the material under consideration. Finally, equation of field intensity has the form-

$$E^{n+1} = \frac{D^{n+1} - \sum_{i=1}^{N} P_i^{n+1}}{\in_0 \in_\infty} \tag{5.10}$$

Where N is the number of poles and D^{n+1} is the next value of electric flux density after one iteration in FDTD algorithm.

Chapter 6

Design of a High Pass Wavelength Filter

6.1 Introduction

Surface plasmon polariton propagates at MIM interface which can be used to design high pass wavelength or low pass frequency filter. Having the simulation algorithm in MATLAB®, the proposed structure transmission efficiency can be found out from which the high pass wavelength characteristics of the proposed structure is proved. For the better performance various designed structure parameters are changes and the parameter which is responsible for the change of cutoff wavelength is found out.

6.2 High Pass Wavelength Filter Structures

The proposed filter design consists of MIM structure with an insulator as a waveguide sandwiched by metal. Air film used as insulator and Silver (Ag) as metal. The waveguide consists of inward grating profile apodized by super Gaussian function. The inward grating profile will allow plasmonic propagation of wavelengths greater than a certain wavelength and attenuate the propagation of wavelengths less than that wavelength. The designed structure is composed of Silver substrate of dimension 1000nm × 1000nm. The waveguide is seen in Fig.3.1 with inward grating profile apodized by super Gaussian function. The width of the waveguide, D is 205nm, the grating length, L is 820nm. The maximum grating width, d is 55 nm and grating period, A is 40nm. Grating period is defined as the distance from starting of a grating to the starting of next grating as shown in Fig.6.1.

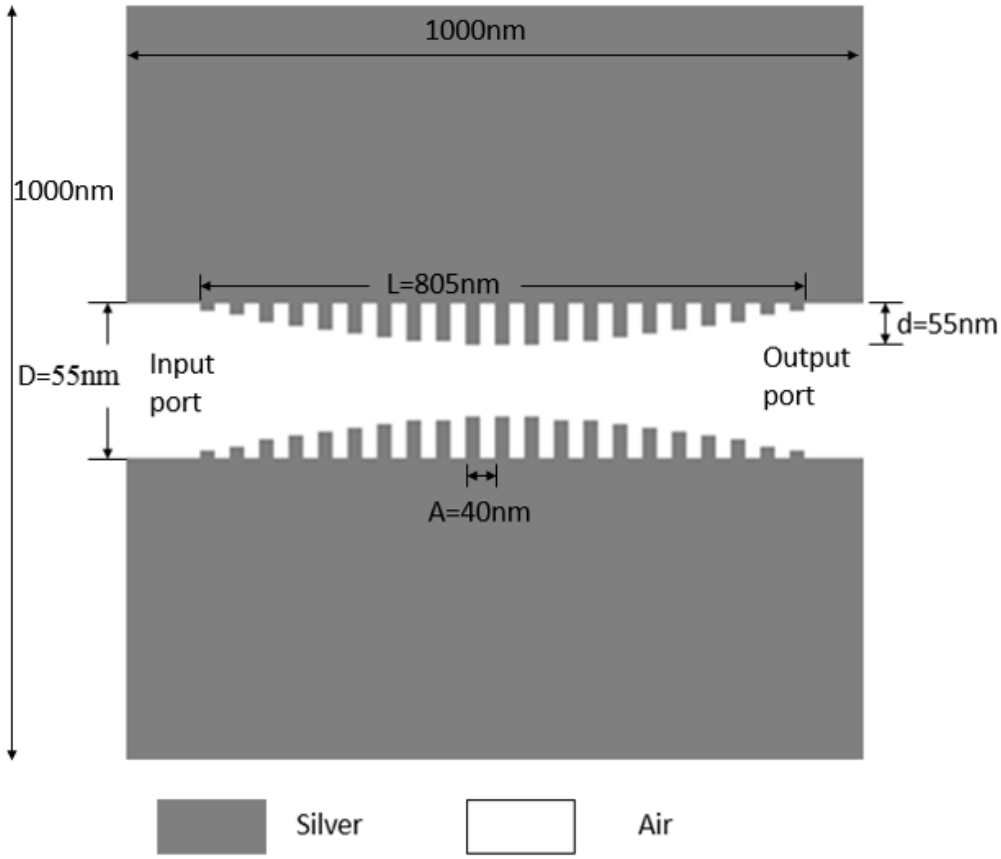

Fig. 6.1: Basic structure of the proposed high pass wavelength filter

Input and outport is assigned to make an analogy with filter performance. The left most part of the waveguide is assigned as input port and right most part is output port. Now, since we've developed the general simulation model for any structure, we can simulate how a plasmonic profile of different wavelength would propagate through the structure.

6.3 Performance analysis

The performance of filter may be referred as how good it is attenuating a certain frequency and passing a certain frequency. Transmittance or transmission efficiency is the appropriate measure of the performance of the filter with its corresponding wavelength. The energy passed through the input port and output port is measured for various wavelength and transmission efficiency is determined by dividing the energy

obtain at output port by input port. The calculations have been done for varying wavelengths of the incident signal. Thus, from the plot of energy measured at the input and output port vs. the wavelength of the incident signal, we can visualize the performance of the filter at different wavelengths.

6.3.1 Calculation of the Energy Passed through the Ports

For the purpose of calculating the energy, firstly the power at the ports for different time steps are calculated. To calculate the power at different time steps, Poynting vector was used. Poynting vector is defined as the cross product of Electric and Magnetic field intensities at a certain instant or here, time step. Mathematically-

$$\vec{S} = \vec{E} \times \vec{H} \tag{6.1}$$

Where,

$\vec{S}$ = Instantaneous power,

$\vec{E}$ = Electric field intensities,

$\vec{H}$ = Magnetic field intensities,

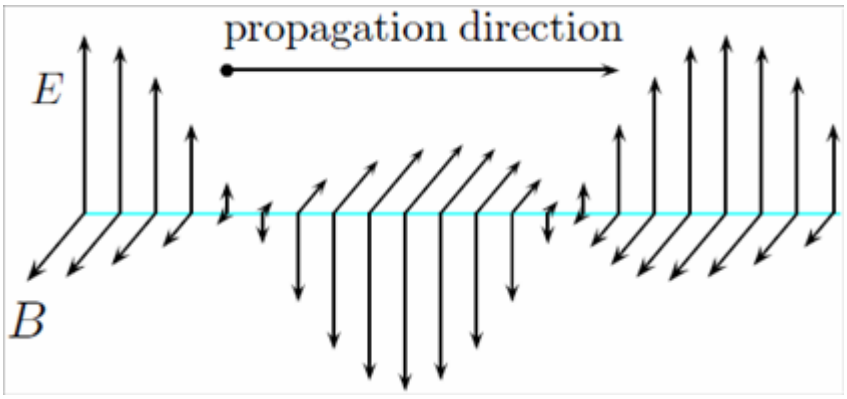

Fig.6.2: E and H fields for calculating instantaneous power.

The power over the range of calculated time steps is found out by multiplying with the time step, we can find out the total energy passed through a particular port for a given no. of time steps. Mathematically, energy passed through will be given by-

$$\text{Energy} = \left|\vec{S}\right| \times \Delta t \tag{6.2}$$

Where, Δt is the time step.

6.4 Performance analysis of the proposed structure

6.4.1 The Energy vs. Wavelength Curve

From the calculation methods described earlier, the obtained energy vs. the wavelength curve for the basic design is as Fig. 6.3.

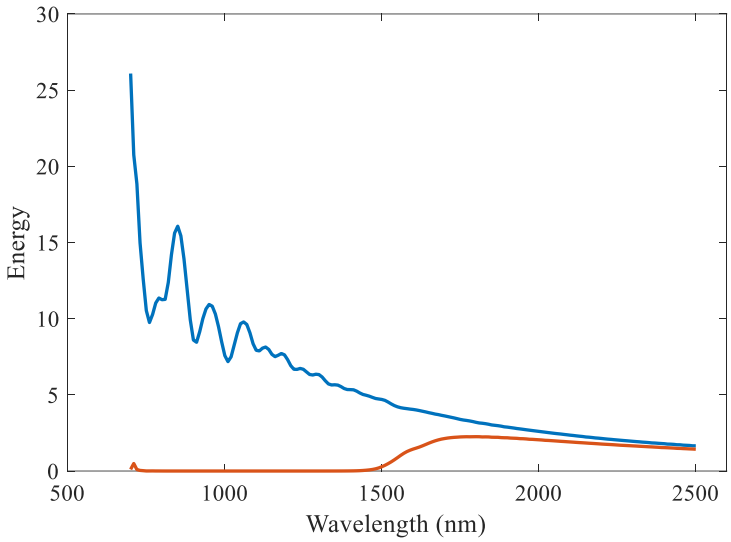

Fig.6.3: Energy vs. wavelength curve

6.4.2 Transmission efficiency vs. Wavelength curve

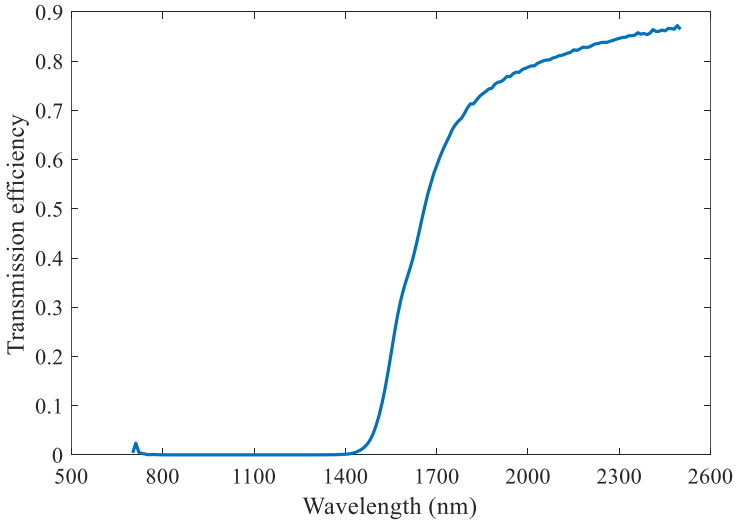

Fig.6.4: Transmission efficiency vs. wavelength curve

6.4.3 Analysis of the curve

This Fig.6.4 shows the performance of the proposed designed filter. As seen from the figure there is no output before wavelength 1420 nm after that the designed structure passes energy at the output in an efficient way. The transmission efficiency rises quite sharply from 0 to 80 percent in the pass band region. The wavelengths for which it doesn't pass energy is known as stop band and the wavelengths for which the energy is passed is called pass band. So, it is working as a high pass wavelength filter or low pass frequency filter. The low cut-off wavelength is 1380 nm or high cut-off frequency is 211.11 THz. To vary the cut-off wavelength or frequency the structure is modified.

6.5 Modification of the proposed structure

6.5.1 Modification by Reducing grating period, A

the grating period, A is reduced to 20 nm from 40 nm. To keep the uniform shape the grating length, L reduced to 810 nm and others parameter remain same

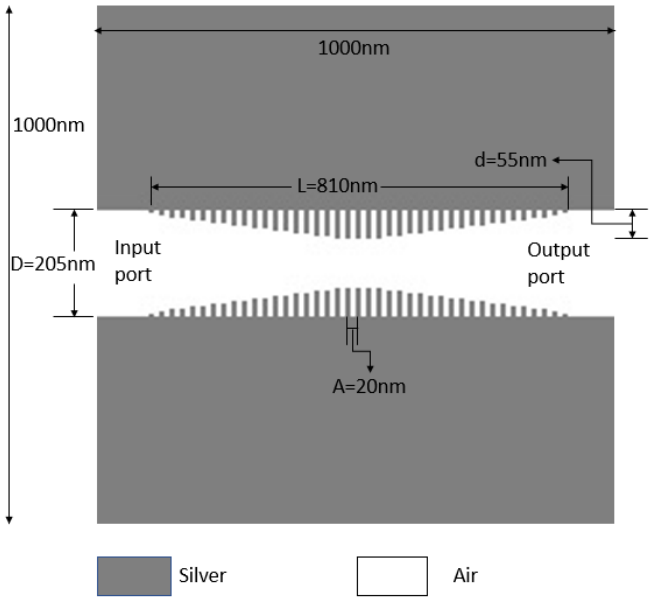

Fig.6.5: Modified structure, Grating period A=20nm

6.5.2 Energy vs. Wavelength Curve of the first modified structure

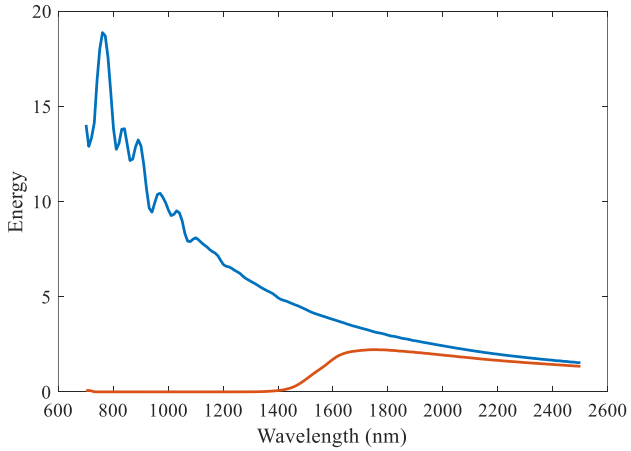

Fig.6.6: Energy vs. wavelength curve of modified structure (A=20nm)

6.5.3 Transmission efficiency vs. Wavelength curve

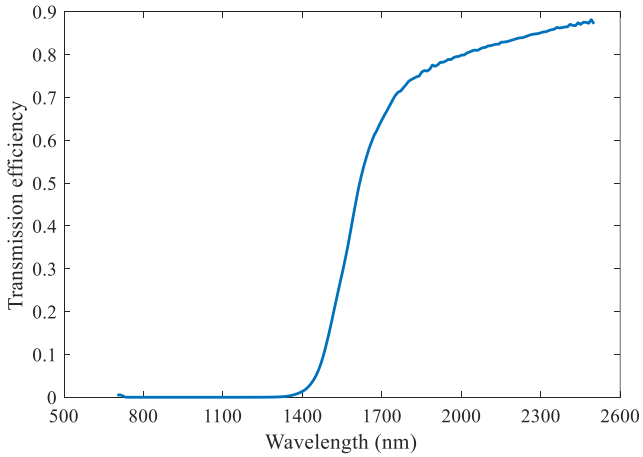

Fig.6.7: Transmission efficiency vs. wavelength curve for the structure with A=20nm

6.5.4 Analysis of the curve

From the energy vs. wavelength curve in Fig6.6 and transmission efficiency vs. wavelength curve in Fig.6.7 it is observed this structure gives a high pass wavelength or low pass frequency filter. And the low cut-off wavelength is 1360 nm and in case of frequency the high cut-off frequency obtain is 220.58 THz.

6.5.5 2nd structure with reducing grating period, A from proposed design

The grating period, A is reduced to 30 nm from 40 nm used in proposed design. For keeping the symmetrical apodized Gaussian grating profile the Grating length, L is reduced to 795 nm. It is shown in the Fig.6.8.

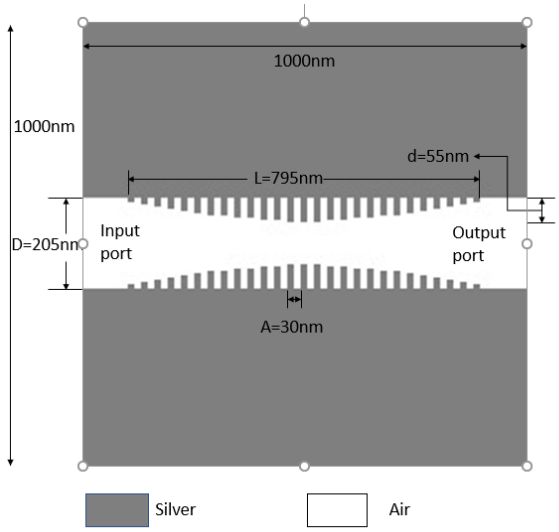

Fig.6.8: 2nd modified structure with grating period, A=30nm

6.5.6 Energy vs. Wavelength Curve of the first modified structure

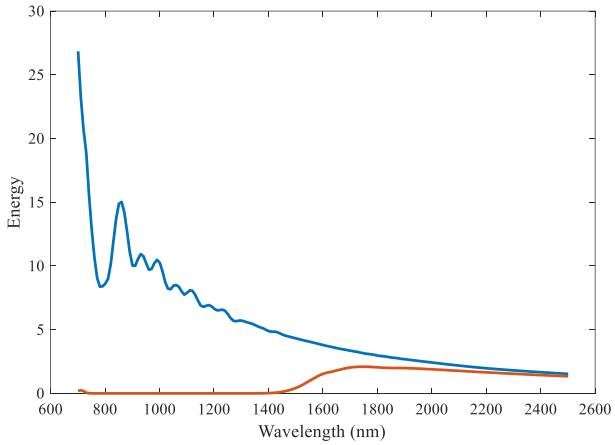

Fig.6.9: Energy vs. wavelength curve of the modified structure with A=30nm

6.5.7 Transmission efficiency vs. Wavelength curve

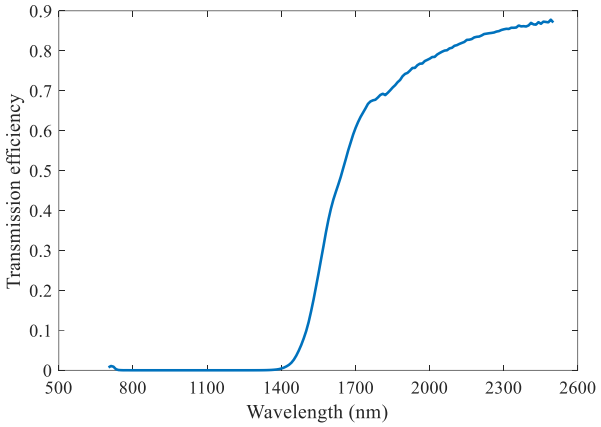

Fig.6.10: Transmission efficiency vs. wavelength curve of the modified structure with A=30nm

6.5.8 Analysis of the curve

The energy and transmission efficiency curve vs. wavelength shows this structure also function as high pass wavelength filter. The low cut-off wavelength of the modified filter is 1390 nm and the corresponding high cut-off frequency is 215.16 THz.

6.6 Comparison of the performance of the modified designed filter

In the Table 6.1 the modified parameter are given with the variation of the cut-off wavelength.

Table 6.1 Structure parameter with different grating period

Structure No.	**Grating period A (nm)**	**Maximum grating width d (nm)**	**Grating length L (nm)**	**Cut-off wavelength λ (nm)**
i	40	55	820	1420
ii	20	55	810	1360
iii	30	55	795	1390

The transmission efficiency of the structures with different parameter is shown in the Fig.6.11. To compare among their performance, the modified structures are numbered as structure i, ii, and iii.

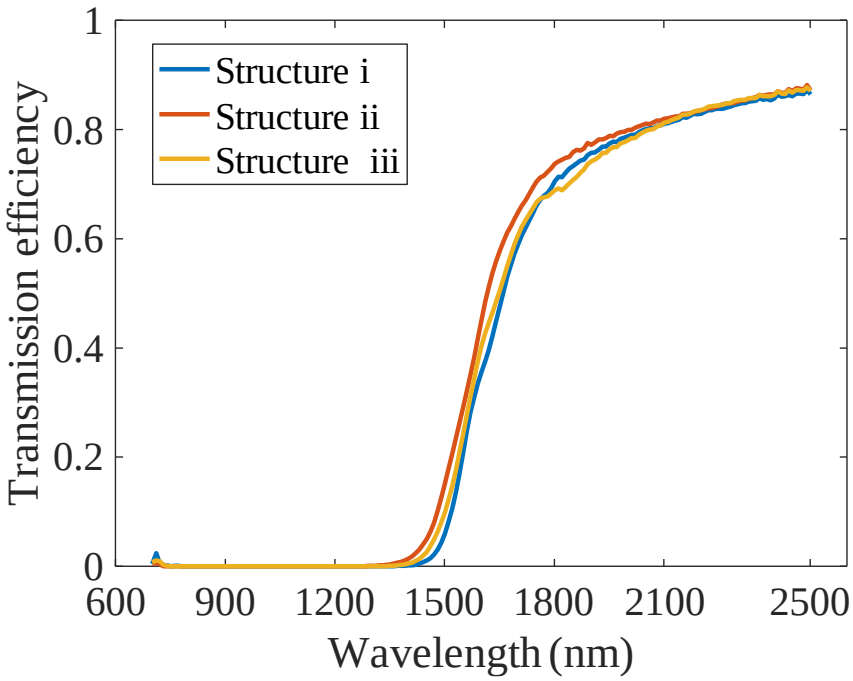

Fig.6.11: Transmission efficiency for different grating period

As seen from the Table 6.1 and observed from Fig.6.11 the low cut-off wavelength of the filter doesn't change significantly with the change of grating period. A new parameter is now considered for varying the cut-off wavelength. In the next section the modification of the structure is done by changing the maximum grating width, d.

6.7 Modified structure by varying the maximum grating width

As the changes in grating period couldn't change the cut-off wavelength significantly so now the modification is done by varying the maximum grating width.

6.7.1 Modified structure reducing the maximum grating width

The all other parameter are kept same only the maximum grating width is reduced to 40 nm from 55 nm with grating length, L of 820 nm and simulation is done like the previous others.

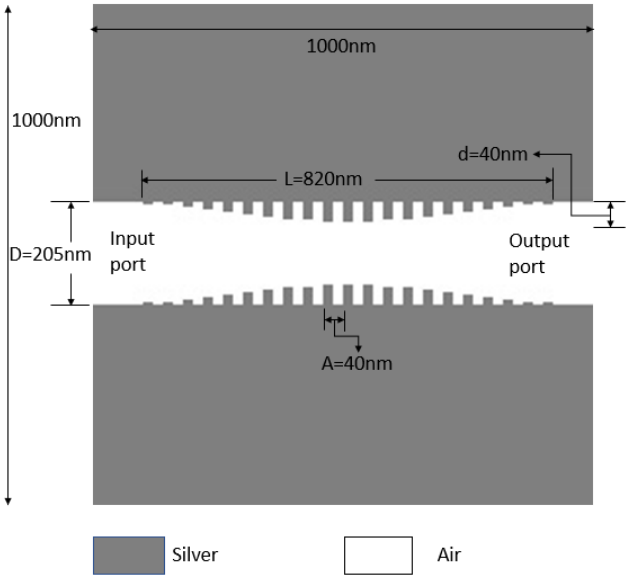

Fig.6.12: Modified structure reducing grating width, d

We have simulated the structure behavior with the developed simulation model.

6.7.2 Energy vs. Wavelength Curve

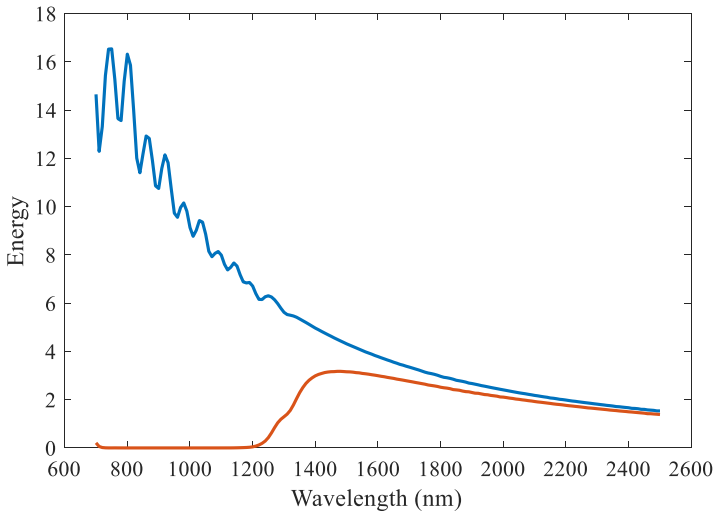

Fig.6.13: Energy vs. wavelength curve for modified structure reducing grating width

6.7.3 Transmission efficiency vs. Wavelength curve

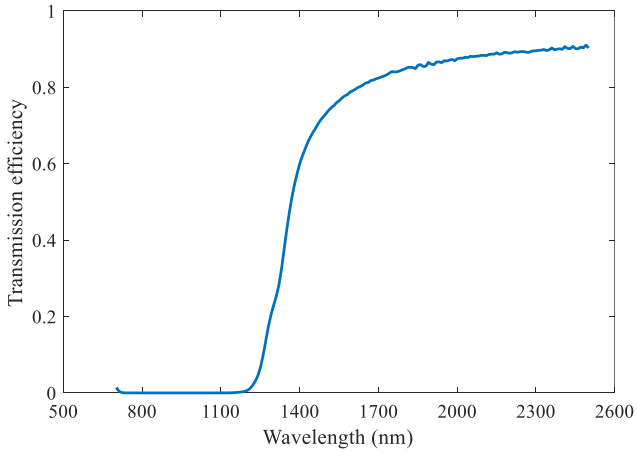

Fig.6.14: Transmission efficiency of the modified structure reducing the grating width

6.7.4 Analysis of the curve

Fig.6.13 and Fig.6.14 shows that the structure also act as high pass wavelength filter like previous structures. The transmission efficiency vs. wavelength curve shows the low cut-off wavelength is 1170 nm and corresponding high cut-off frequency is 256.41 THz. With the decrease of the maximum grating width the high cut-off wavelength of the filter is also decreased.

6.7.5 Modified structure with maximum grating width of 70 nm

The grating width, d is increased to 70 nm keeping all other parameter same.

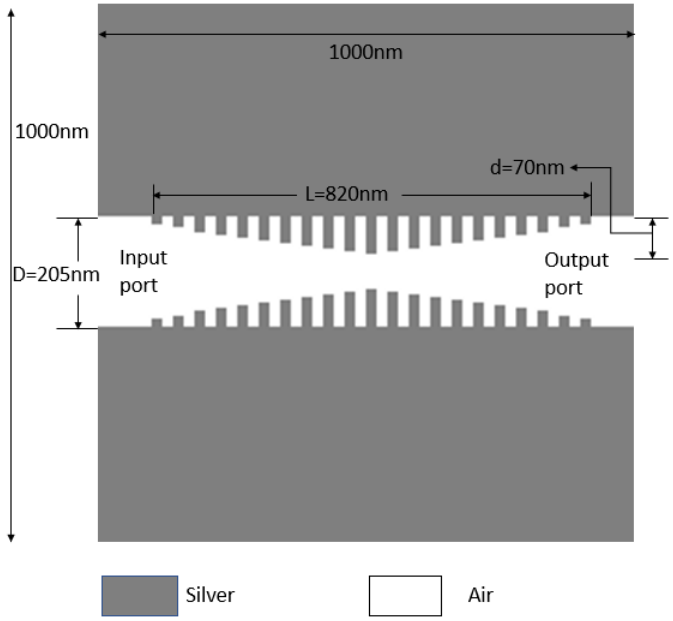

Fig.6.15: Modified structure increasing grating width, (d=70nm)

6.7.6 Energy vs. Wavelength Curve

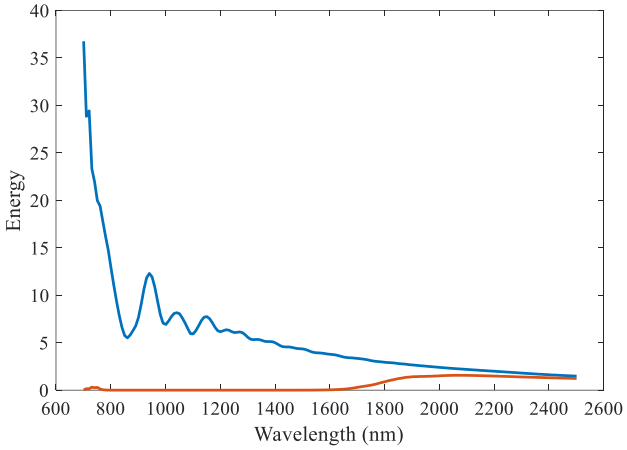

Fig.6.16: Energy vs. wavelength curve with grating width of 70 nm

6.7.7 Transmission efficiency vs. Wavelength curve

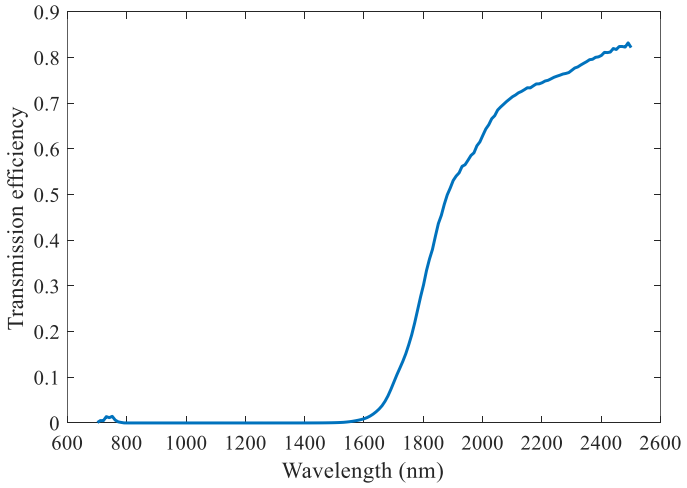

Fig.6.17: Transmission efficiency of the modified structure with grating width of 70nm

6.7.8 Analysis of the curve

The transmission efficiency curve shows that there is increase of high cut-off wavelength of the filter due to increase of maximum grating width. Here the low cut-off wavelength of the filter is 1560 nm and corresponding high cut-off frequency is 192.30 THz.

6.7.9 Third modified structure increasing the maximum grating width

The grating width is further increased to 85 nm and performance of the filter is simulated with developed simulation model.

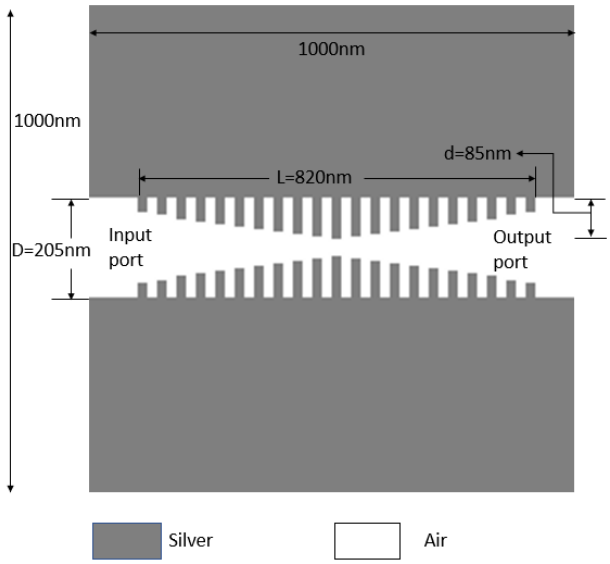

Fig.6.18: Modified structure with maximum grating width of 85 nm

6.7.10 Energy vs. Wavelength Curve

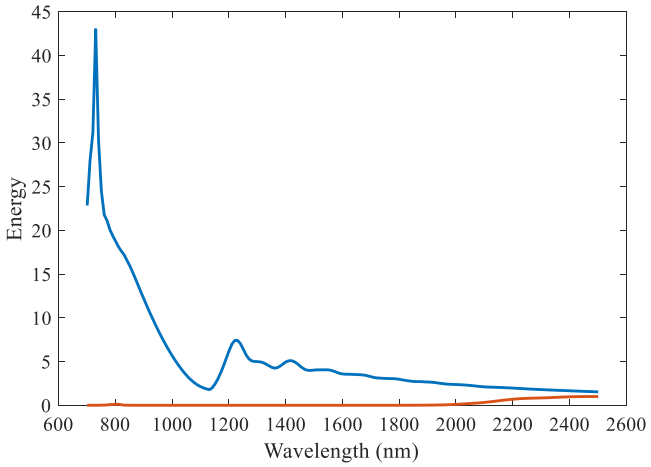

Fig.6.19: Energy vs. wavelength curve of the modified structure

6.7.11 Transmission efficiency vs. Wavelength curve

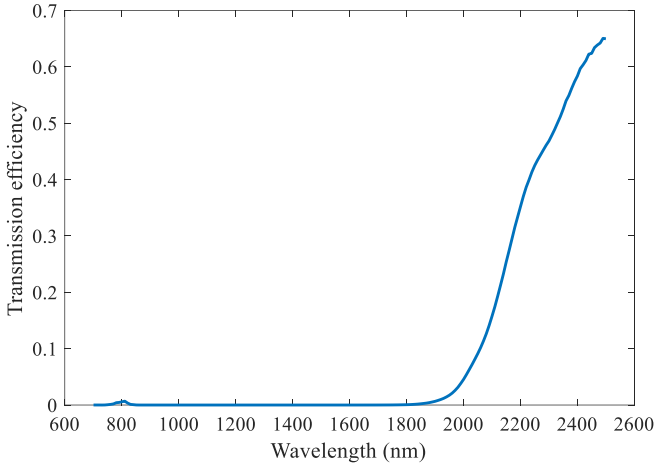

Fig.6.20: Transmission efficiency of the modified structure

6.7.12 Analysis of the curve

As the maximum grating width increased further the low cut-off wavelength increased with it. The low cut-off wavelength of the filter is 1880 nm and corresponding high cut-off frequency is 159.57 THz.

6.8 Comparison of the modified structure performances with variation of grating width

The variation of the parameter used in the structures is given in Table 6.2 and the corresponding cut-off wavelength is also mentioned and structure number is used for better understanding of the comparison.

Table 6.2 Inward grating varying grating width, d

Structure No.	**Grating period A (nm)**	**Maximum grating width d (nm)**	**Grating length L (nm)**	**Cut-off wavelength λ (nm)**
i	40	55	820	1420
iv	40	40	820	1170
v	40	70	820	1560
vi	40	85	820	1880

In Fig.6.21 the performance of the different structure is shown and from the figure it is observed that the low cut-off wavelength of the filter changes significantly with the changes of maximum grating width. And the changes are directly proportional to the increase or decrease of the grating width, i.e the increase of maximum grating width increases the low cut-off wavelength of the filter and vice-versa.

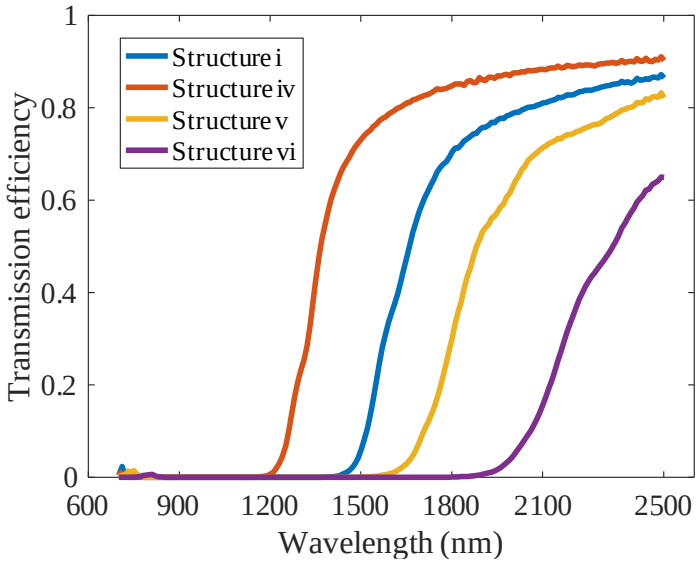

Fig.6.21: Transmission efficiency of the different modified structure

6.9 Modified structure with outward grating profile

Now to observe the effect of outward grating profile instead of inward grating profile the structures are modified accordingly with outward grating profile.

6.9.1 Modified structure of the proposed design by outward grating profile

The parameters used are all same as the design parameter of the inward grating profile. The silver substrate is of dimension 1000nm × 1000nm. Width of the waveguide is 205 nm, grating length 820 nm, grating period of 40 nm and maximum grating width of 550nm.

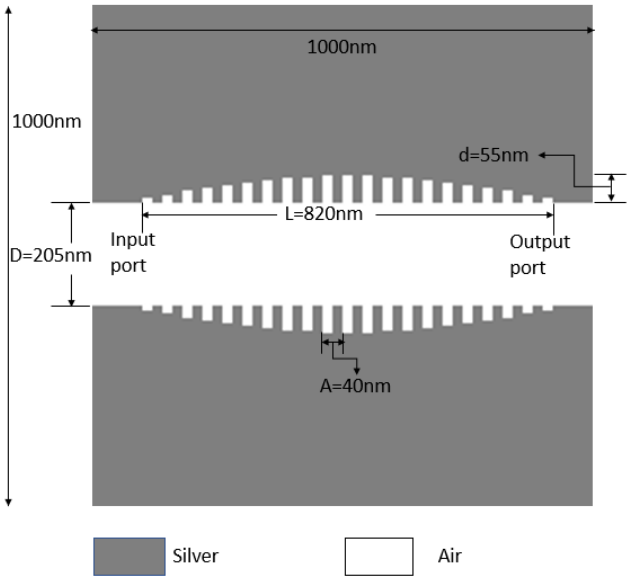

Fig.6.22: Modified structure with outward grating profile

The performance of the modified structure is found by simulating with the developed simulation model.

6.9.2 Energy vs. Wavelength Curve

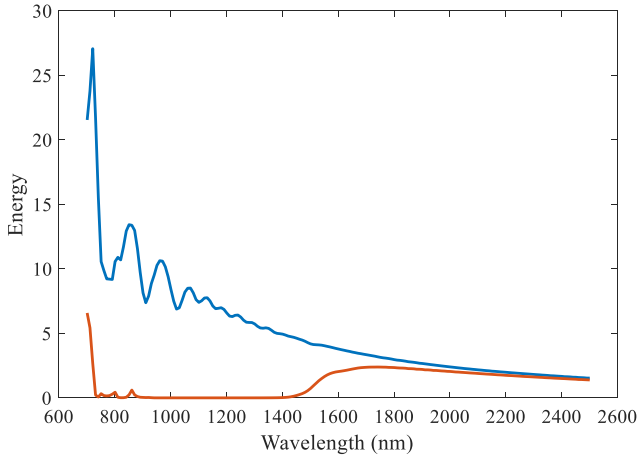

Fig.6.23: Energy vs. wavelength curve of the structure with outward grating profile

6.9.3 Transmission efficiency vs. Wavelength curve

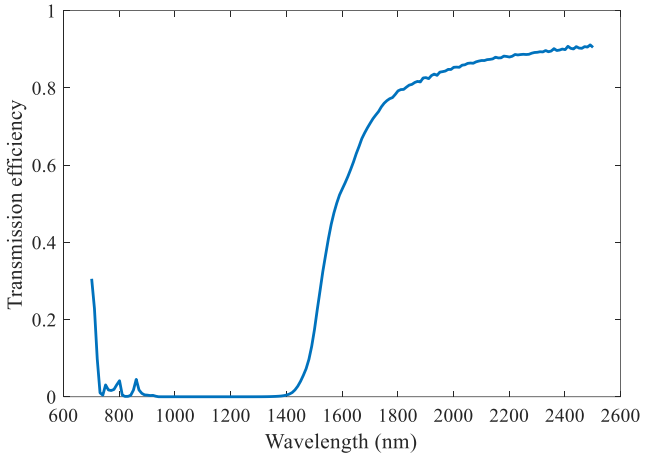

Fig.6.24: Transmission efficiency vs. wavelength of the structure with outward grating profile

6.9.4 Analysis of the curve

Fig.6.24 shows the transmission efficiency of the modified structure of the designed filter with outward grating profile apodized by super Gaussian function. Performing as high pass wavelength filter, the low cut-off wavelength is 1390 nm and corresponding high cut-off frequency is 215.83 THz.

6.9.5 Modified structure reducing grating width of outward grating profile

The grating period doesn’t affect significantly the cut-off wavelength so modification is not done by changing the grating period anymore. The maximum grating width is reduced to 40 nm of outward grating profile shown in Fig.6.25.

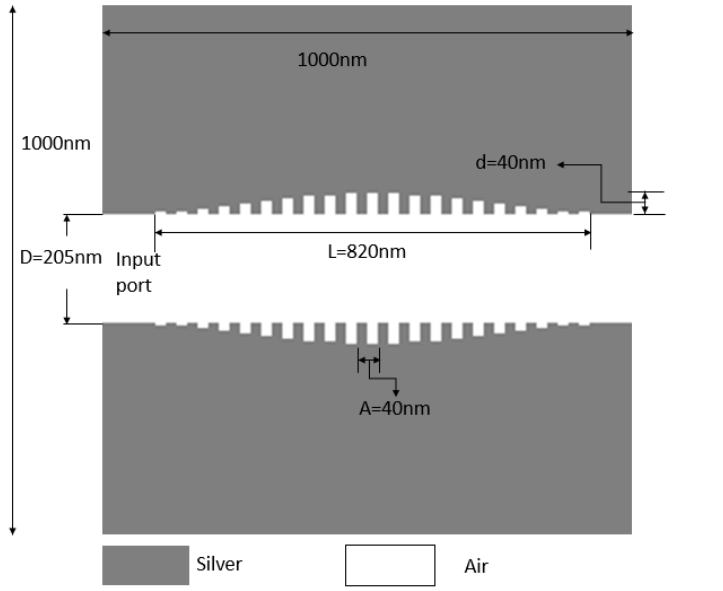

Fig.6.25: Modified structure reducing maximum grating width of outward grating profile

6.9.6 Energy vs. Wavelength Curve

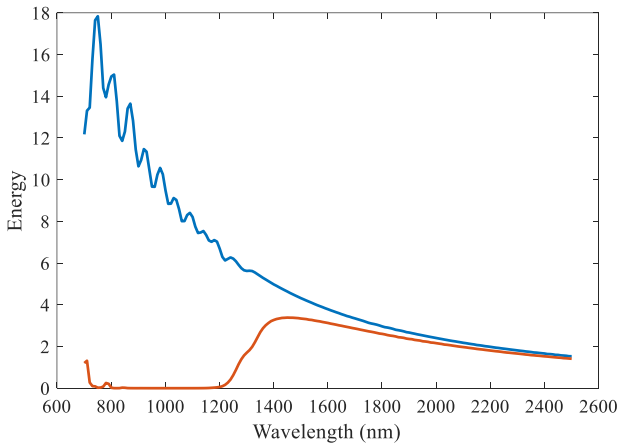

Fig.6.26: Energy vs. wavelength curve of modified structure

6.9.7 Transmission efficiency vs. Wavelength curve

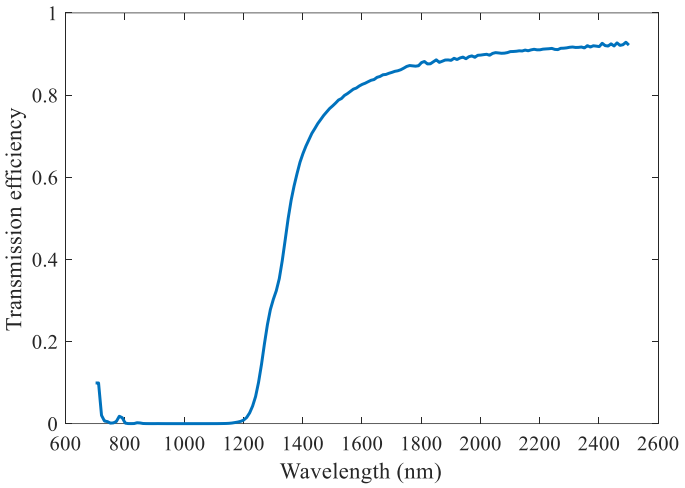

Fig.6.27: transmission efficiency of modified structure reducing grating width of outward grating profile

6.9.8 Analysis of the curve

The curve shows a high pass wavelength characteristics and the low cut-off wavelength is 1180 nm corresponding to high cut-off frequency of 254.23 THz.

6.9.9 Modified structure increasing grating width of outward grating profile

The grating width is increased to 70 nm keeping all other parameter same as before

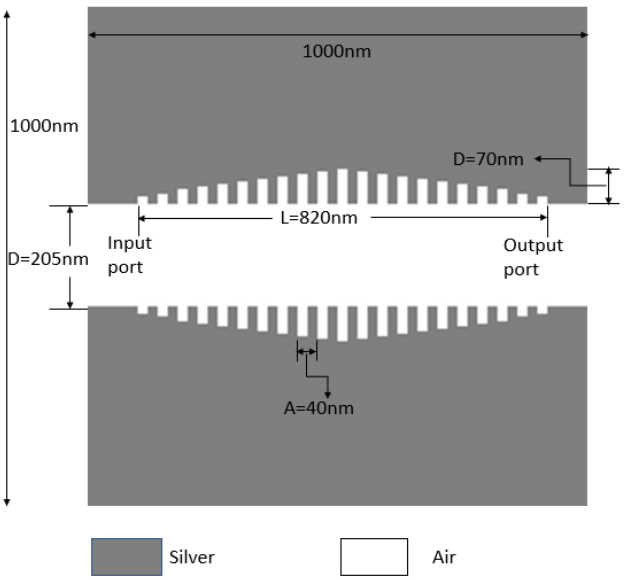

Fig.6.28: Modified structure increasing max grating width

6.9.10 Energy vs. Wavelength Curve

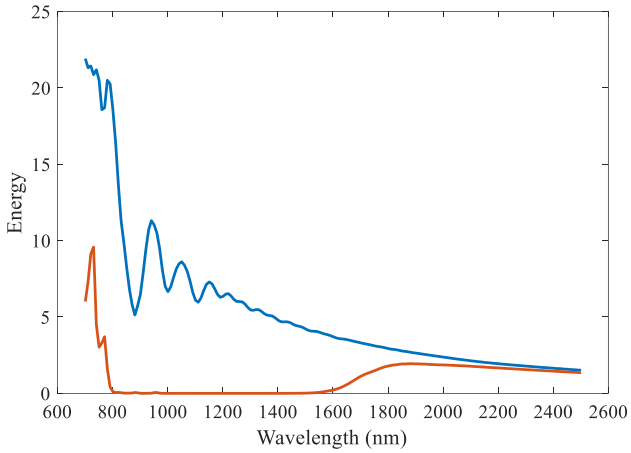

Fig.6.29: Energy vs. wavelength curve of the structure increasing grating width

6.9.11 Transmission efficiency vs. Wavelength curve

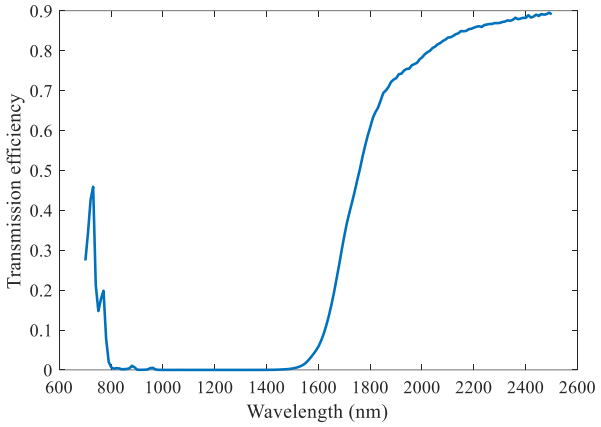

Fig.6.30: Transmission efficiency of the modified structure increasing grating width

6.9.12 Analysis of the curve

From the transmission efficiency of the structure shown in Fig.3.29 the low cut-off wavelength of the high pass wavelength filter design is 1490 nm and the corresponding high cut-off frequency is 201.34 THz.

6.9.13 Modified structure with outward grating profile further increasing maximum grating width

The maximum grating width is increased to 85 nm keeping all other parameter same in the modified design of filter by outward grating profile.

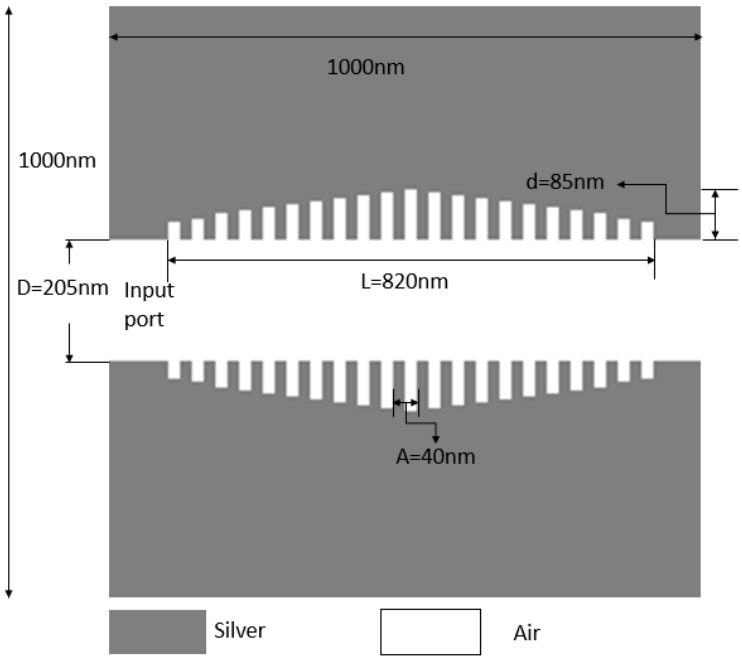

Fig.6.31: Modified structure increasing max grating width

6.9.14 Energy vs. Wavelength Curve

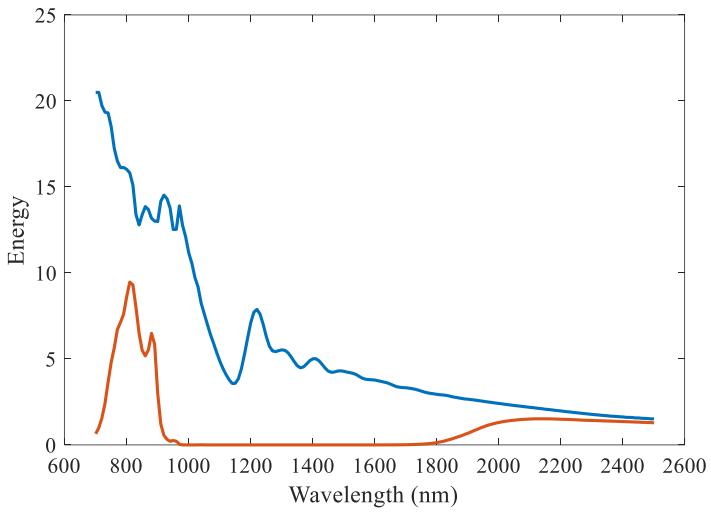

Fig.6.32: Energy vs. wavelength curve of the modified filter structure

6.9.15 Transmission efficiency vs. Wavelength curve

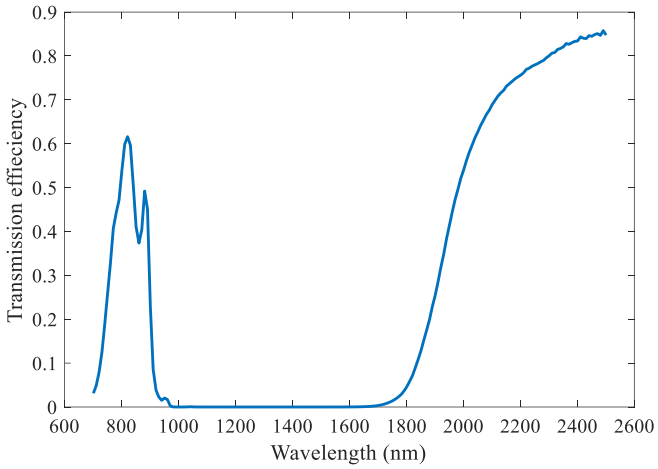

Fig.6.33: Transmission efficiency vs. wavelength the modified structure increasing grating width

6.9.16 Analysis of the curve

The transmission efficiency showing it as a high pass wavelength filter and the low cut-off frequency is 1750 nm and the corresponding high cut-off frequency is 171.43 THz.

6.10 Comparison among the modified structure by outward grating profile

In the Table 6.3 the parameter changes are given corresponding to its structure.

Table 6.3 Outward grating varying grating width, d

Structure No.	**Grating period A (nm)**	**Maximum grating width d (nm)**	**Grating length L (nm)**	**Cut-off wavelength λ (nm)**
vii	40	55	820	1390
viii	40	40	820	1180
ix	40	70	820	1490
x	40	85	820	1750

The transmission efficiency of different structure is shown in Fig.6.34 and from here it is observed that these are high pass wavelength filter and the low cut-off wavelength

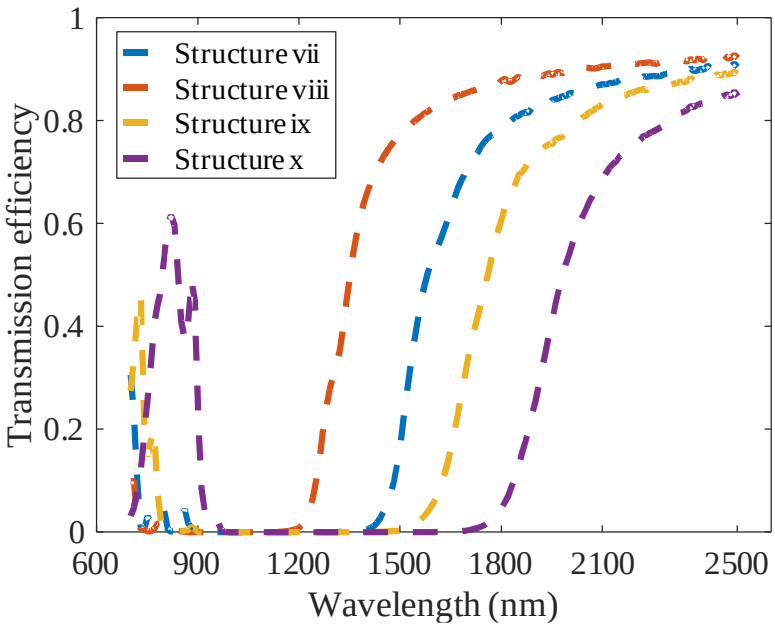

Fig.6.34: Transmission efficiency of the designed structures with outward grating profile

varies significantly with the variation of the maximum grating width and is directly proportional to the changes of the cut-off wavelength, i.e the low cut-off wavelength decreases with the decrease of maximum grating width and vice-versa.

6.11 Comparison with the inward and outward grating profile

Now the comparison among the structure designed by both inward and outward grating profile is made. In Table 3.4 the all parameters are shown with their corresponding structure and the cut of frequency is also given.

Table 3.4 Comparison between Inward and Outward grating

Structure No.	**Grating period A (nm)**	**Maximum grating width d (nm)**	**Grating length L (nm)**	**Grating type**	**Cut-off wavelength λ (nm)**
i	40	55	820	Inward	1420
vii	40	55	820	Outward	1390
iv	40	40	820	Inward	1170
viii	40	40	820	Outward	1180
v	40	70	820	Inward	1560
ix	40	70	820	Outward	1490
vi	40	85	820	Inward	1880
x	40	85	820	Outward	1750

The transmission efficiency of the structures are shown in Fig.3.34 and from the transmission it is observed that with the variation of maximum grating width the corresponding cut-off wavelength changes significantly in both inward and outward grating profile and is directly proportional to the changes. In the Fig.3.34 the solid line represents the performance of structure by inward grating profile and dotted line represent the outward grating profile. Here with the increase of maximum grating width the low cut-off wavelength also increases and decreases with decreasing of maximum grating width. So from here it is determined that the grating width changes the cut-off wavelength significantly which can’t be obtained by the variation of grating period.

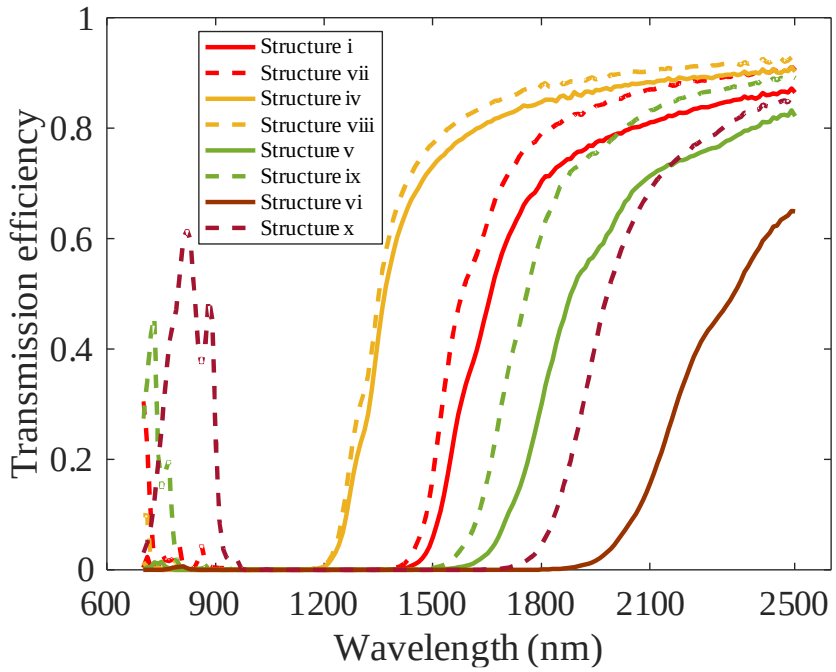

Fig.6.35: Transmission efficiency of different structure with both inward and outward grating profile

6.12 Summary

A nanoplasmonic high pass wavelength or low pass frequency filter is proposed. Both inward and outward grating, apodized by super Gaussian function, is used with MIM waveguide and simulated using FDTD method in MATLAB® software by developed simulation model. It is observed that only grating period has a notable effect on the cut-off wavelength. Other parameters have no significant effect. Cut-off wavelength is almost same for inward and outward grating profiles provided other parameters are kept constant for both profiles. The simulation results of transmission efficiencies give an opportunity to utilize these proposed designs into fabrication of devices.

Chapter 7

Designing band pass filters & Analyzing their performances

7.1 Introduction

Ring resonators are promising building blocks for photonic integrated circuits. A ring resonator can only attenuate a certain band of frequency. So, it can only be used to make band pass filters. At resonance destructive interference occurs & no light can pass through it. So, this also makes it a notch filter. In modern times ring resonators have become an attractive field of research. But most of the works are done on circular ring resonators. Rectangular, elliptical & curved rectangular ring structures are designed here. Different parameters of these structures were varied & comparison between them are made in the preceding sections.

7.2 Band pass filter structures

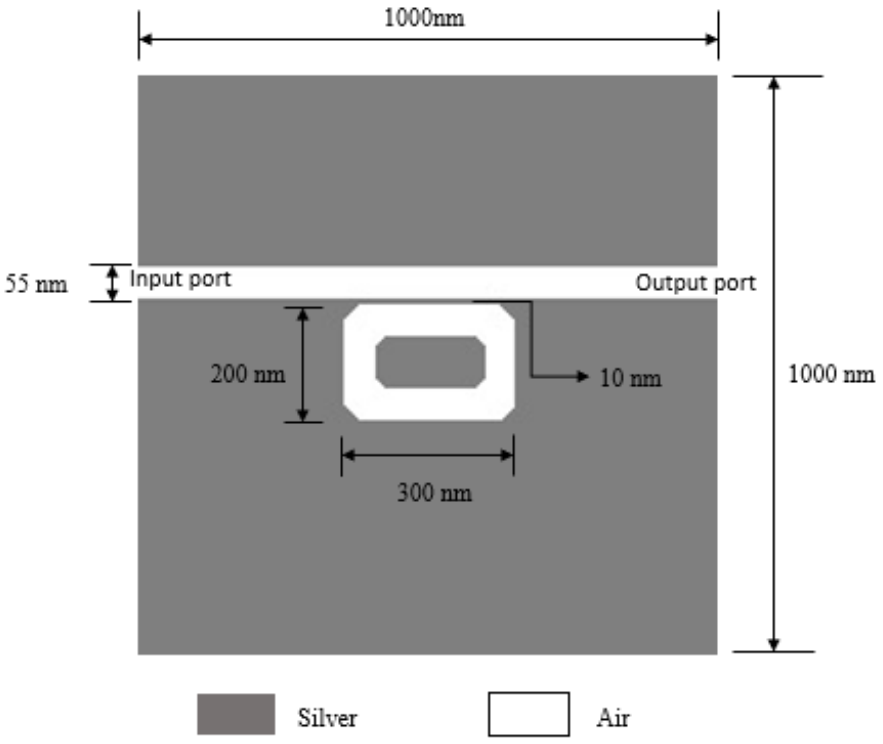

Fig. 7.1: First curved rectangular ring structure

7.2.1 Curved Rectangular ring structures

The structure is composed of 1000nm x 1000nm silver substrate. The white & gray areas denote consecutively air & silver. The width of the air film is 55nm. The curved rectangular ring has a length of 300nm & width of 200nm. The distance between the waveguide & ring is 10nm. The leftmost point is denoted as input port & the rightmost point is denoted as output port. Now after developing the curved rectangular structure, simulation of this can be done in a 2D simulator using FDTD.

7.2.2 Performance Analysis of the designed structure

After designing the proposed structure, it was then simulated using the methods described above. The transmission efficiency vs wavelength curve is shown below. The wavelength considered for the studies was from 700nm-2500nm. The curved line represents the energy passed through the output port. For the wavelength range of 140nm-2400nm the transmission efficiency is close to 80%. This range can be considered as the band pass range. The other regions of the curve have very low efficiency. There are three frequencies where the efficiency is close to 0. They are at approximately 800nm, 1040nm & 2400nm. But they are not ideal notch frequencies because the efficiency is not zero at those points. The modes at high transmittance are shown below. The modes are taken at the three peaks which are approximately at 930nm, 1170nm & 2070nm. These are all odd higher modes. The N number of nodes in the magnetic field distribution within the resonator refers to mode (N-1).

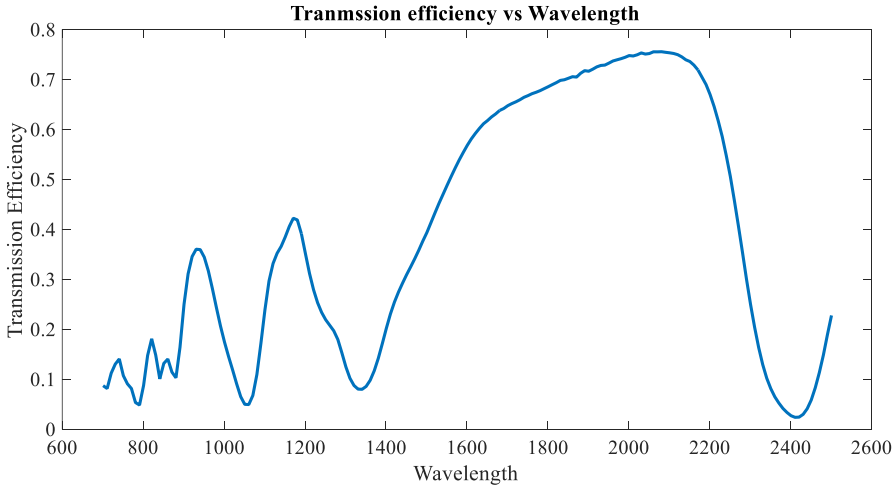

Fig. 7.2: Transmission Efficiency vs Wavelength curve for the first curved rectangular ring structure

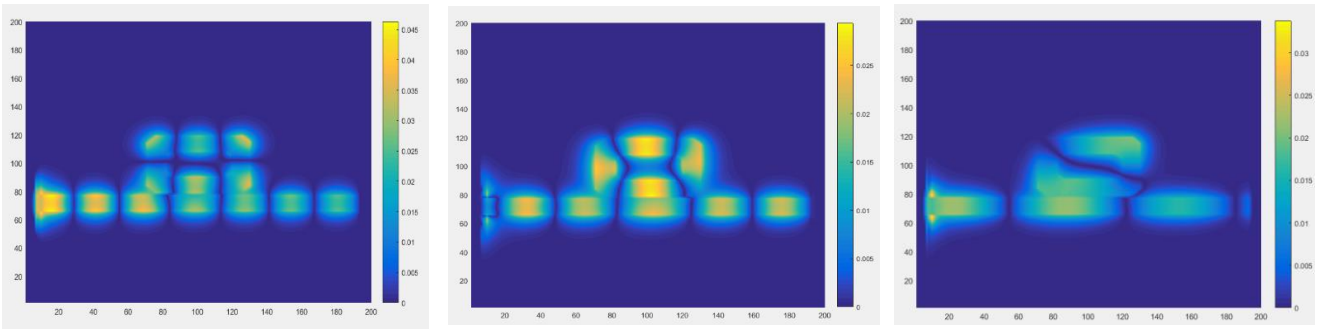

(a) (b) (c)

Fig. 7.3: Mode 5, 3 and 1 at wavelengths a) 930nm, b) 1170nm and c) 2070nm respectively

7.2.3 Second Curved Rectangular Ring Structure

Then the parameters were varied & change in output due to the parameter changes were observed. The length & width of the curved rectangular structure was varied. The length of the curve was changed to 500nm from 300nm & the width was changed to 350nm from 200nm. All the other parameters were kept same. Due to modifications done in the structure the output changed & it can be seen in the next section.

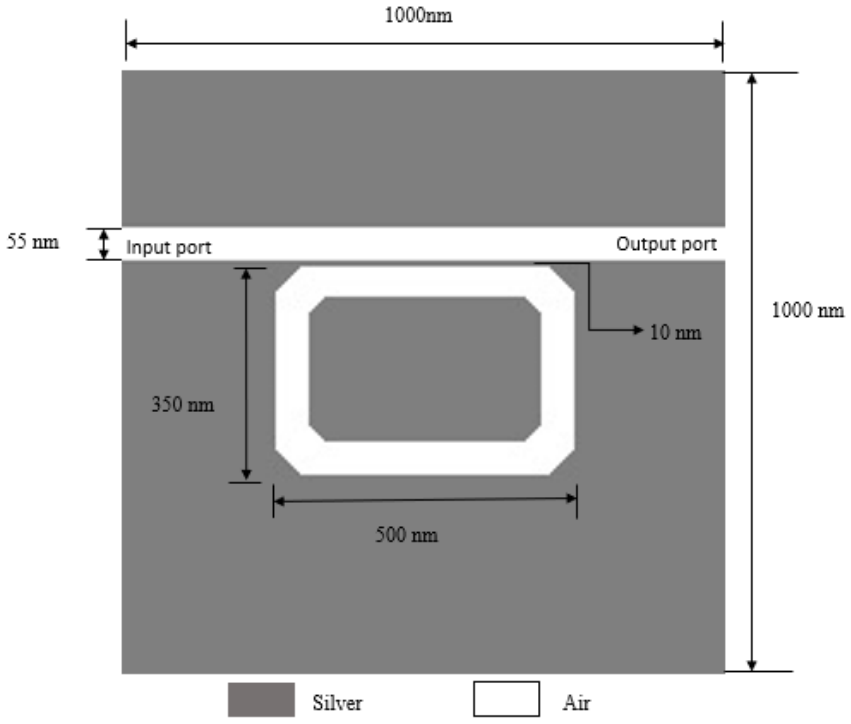

Fig. 7.4: Second curved rectangular ring structure

7.2.4 Performance Analysis of the Structure

The second structure was simulated using the same method & the curve shown below was found. The efficiency of the band pass region has decreased slightly than the previous structure. For this case it is close to 70%. The band pass region has also become narrower. The band pass region for this structure is 1650nm-2400nm as can be seen from the graph below. Two notch frequencies can be observed from the graph. One is around 900nm & the other one is around 2400nm. The modes of high transmittance are shown below. These are also all higher odd modes. The modes are at peak 1040nm, 1170nm & 2080nm.

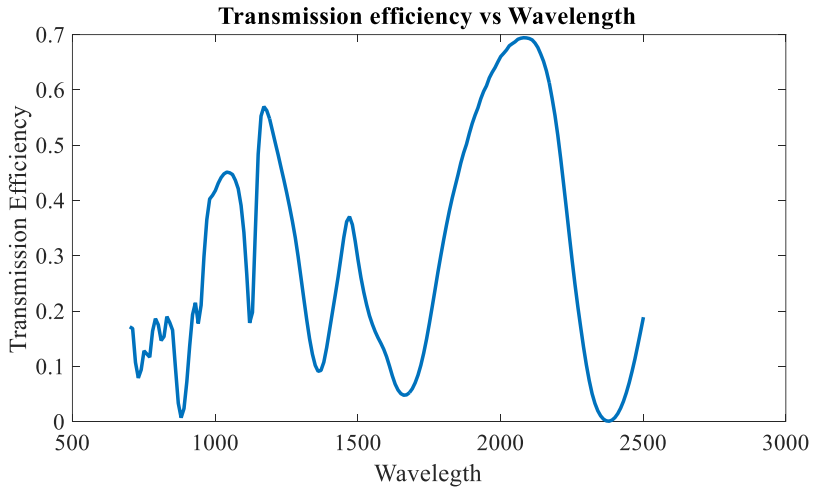

Fig. 7.5: Transmission Efficiency vs Wavelength curve for the second curved rectangular ring structure

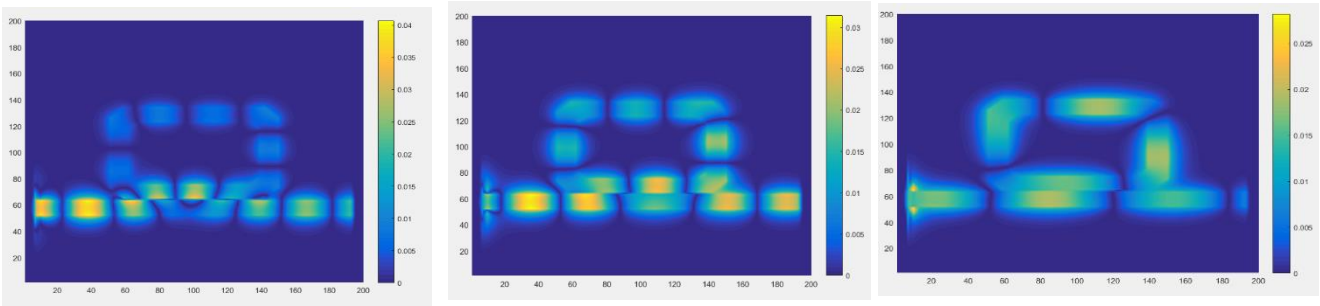

(a) (b) (c)

Fig. 7.6: Mode 9,7 and 3 at wavelengths a) 1040nm, b) 1170nm and c) 2080nm respectively

7.2.5 Elliptical ring structures

The geometric shape of the ring was changed to an ellipse. This structure is also composed of 1000nm x 1000nm silver substrate like the prior ones. The left & right ports are denoted as input & output ports. The structure of the ellipse can be changed by changing the eccentricity. Eccentricity of the ellipse depends on the semi major axis a & semi minor axis b. Because e= $\sqrt{(1-\frac{a^2}{b^2})}$. In this structure the length of the ellipse is 500nm & width is 350nm. The distance between the ring & waveguide is 10nm. The waveguide is sandwiched within the silver substrate. The simulation of this structure was then done accordingly to the previous ones.

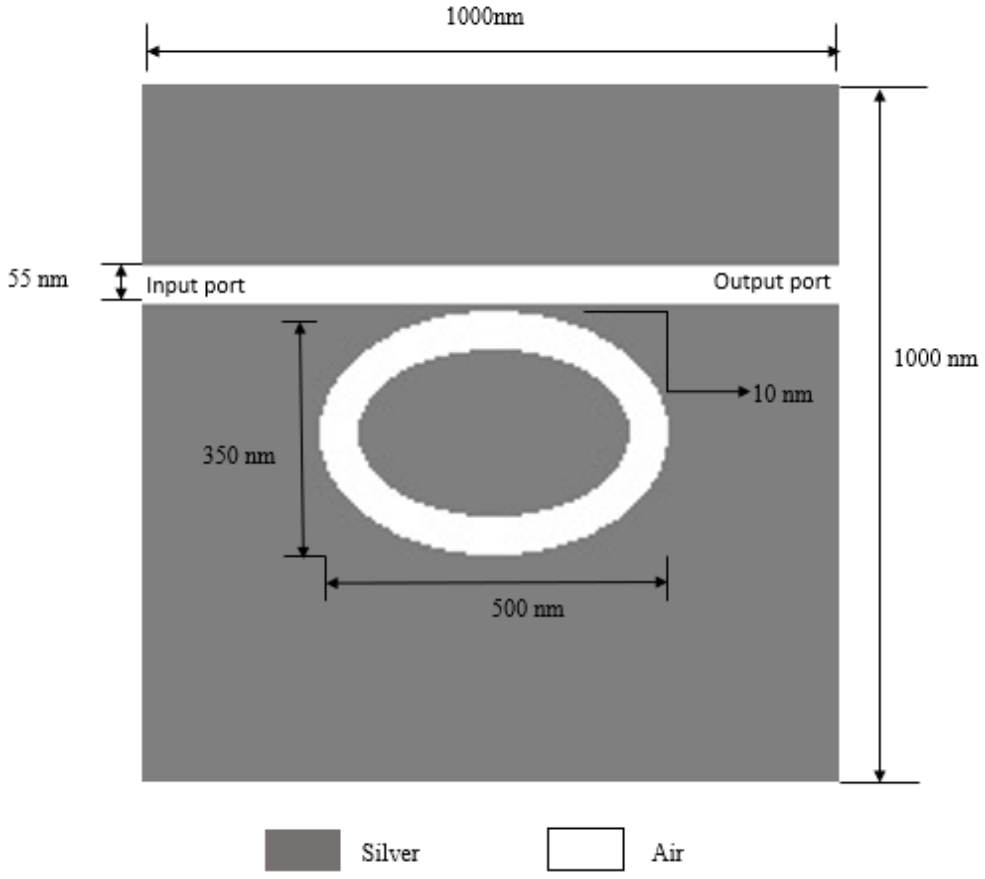

Fig. 7.7: First elliptical ring structure

7.2.6 Performance Analysis of the Structure

After simulating the structure, the transmission efficiency vs bandwidth curve was obtained which is shown below. The maximum transmission efficiency of this structure is 70%. Two notch frequencies were obtained which are approximately at 850nm & 1380nm. But these two frequencies are not perfect notch because the efficiency is not exactly 0 at those points. The FSR observed in this curve is not periodic. If the structure were a perfect ring then the FSR would have been periodic. The maximum transmission efficiency observed in the curve is 78%. Modes at the peak are shown below. These are all high odd modes.

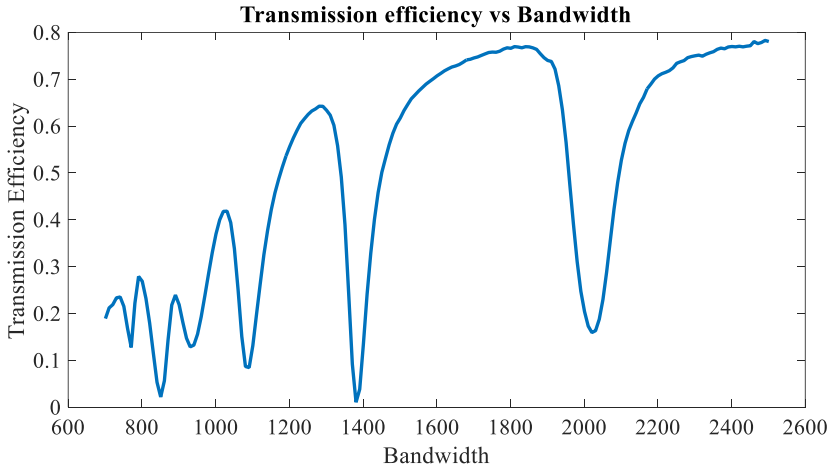

Fig. 7.8: Transmission Efficiency vs Wavelength curve for the first elliptical ring structure

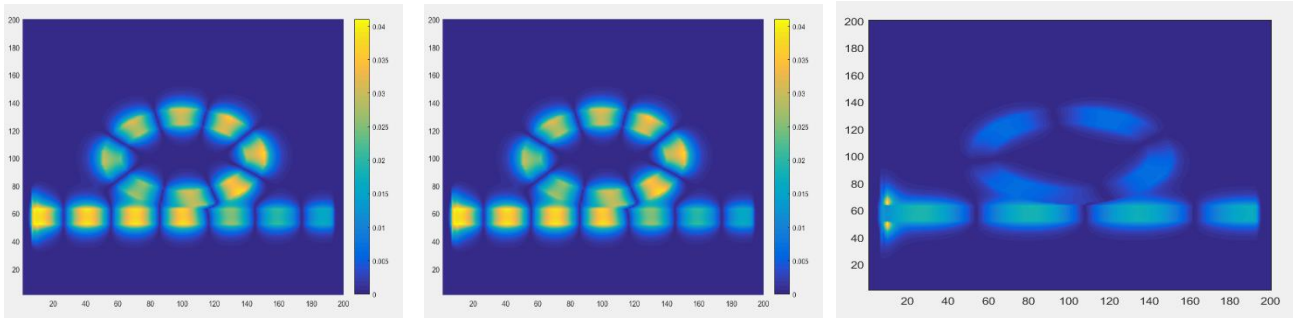

(a) (b) (c)

Fig. 7.9: Mode 7, 5 and 3 at wavelengths a) 1030nm, b) 1210nm and c) 1810nm respectively

7.2.7 Second Elliptical Ring Structure

All the parameters of the structure were kept same as previous. Only the elliptical ring was rotated 90 degrees. Then the structure was given through similar simulations as the previous cases & the plasmon propagation the structure was seen. The output was found out & the transmission efficiency was found out.

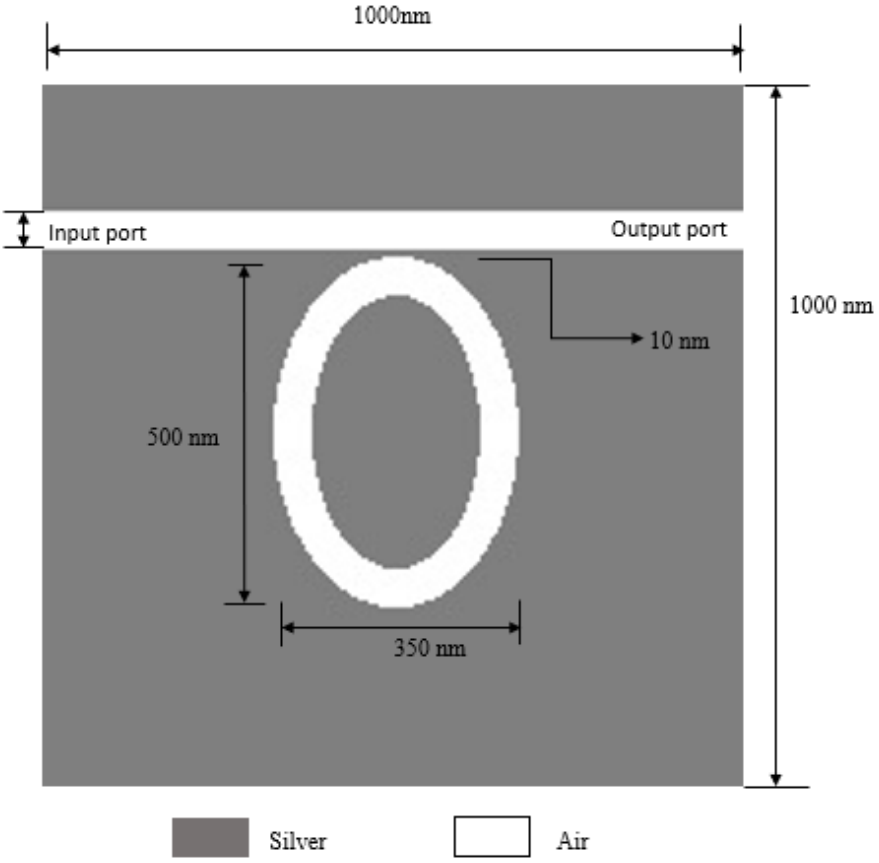

Fig. 7.10: Second elliptical ring structure

7.2.8 Performance Analysis of the Structure

Three notch frequencies were obtained where the efficiency is less than 5%. for band pass. The band pass range can be observed from 1400nm-2050nm. In this range the efficiency is close to 80%. So, the efficiency is almost as same as the previous structure. But the FSRs are different. The FSRs are also aperiodic for this case. The modes at peak 870nm, 1020nm, 1280nm, 1840nm & 2480nm. These are all higher odd modes.

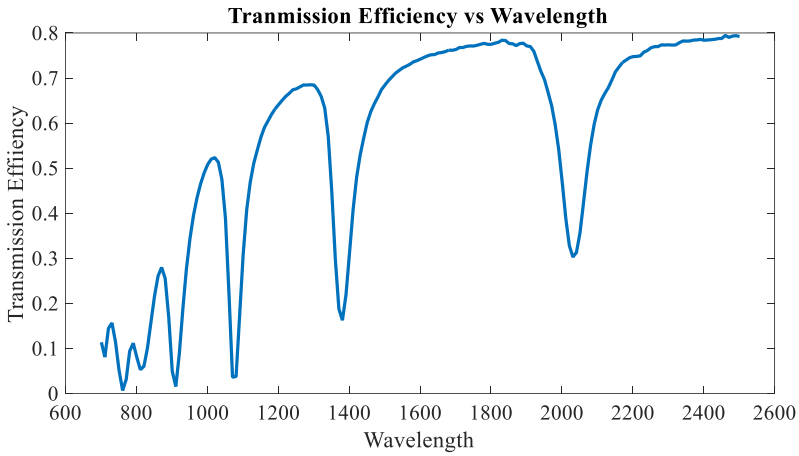

Fig. 7.11: Transmission Efficiency vs Wavelength curve for the second elliptical ring structure

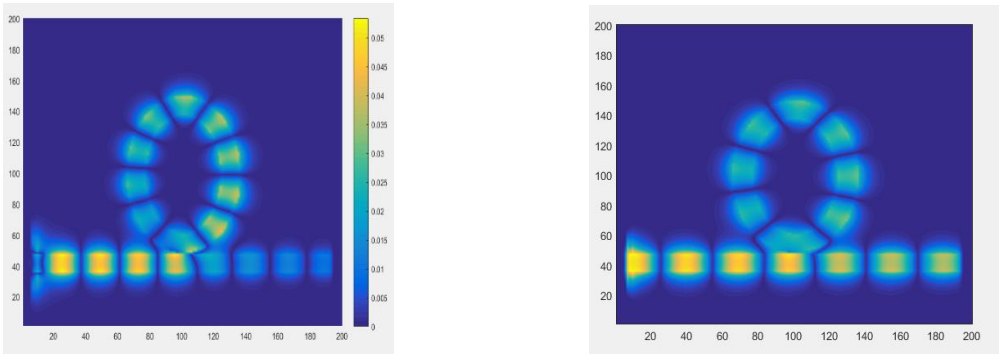

(a) (b)

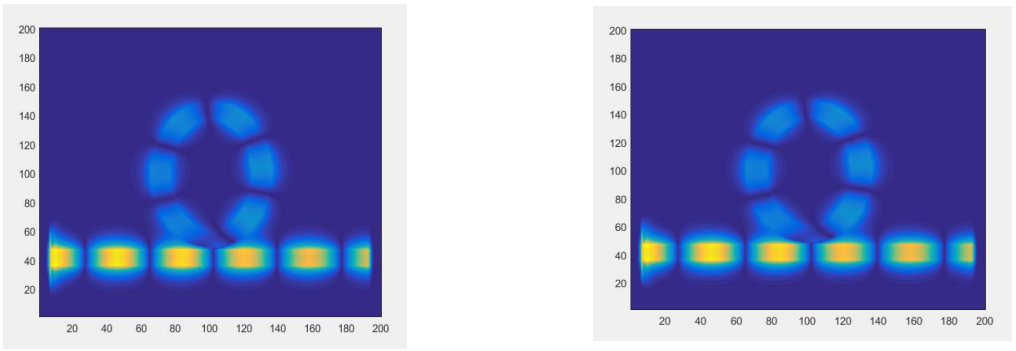

(c) (d)

Fig. 7.12: Mode 9,7, 5 and 3 at wavelengths a) 870nm, b) 1020nm, c) 1280nm and d) 1840 respectively

7.2.9 Third Elliptical Ring Structure

Then the eccentricity of the elliptical ring was changed. Then the length of the ring became 600nm instead of 500nm. All other parameters were also remained unchanged. After making the structure similar simulations were done just like the previous cases. The transmission efficiency of the structure was then plotted.

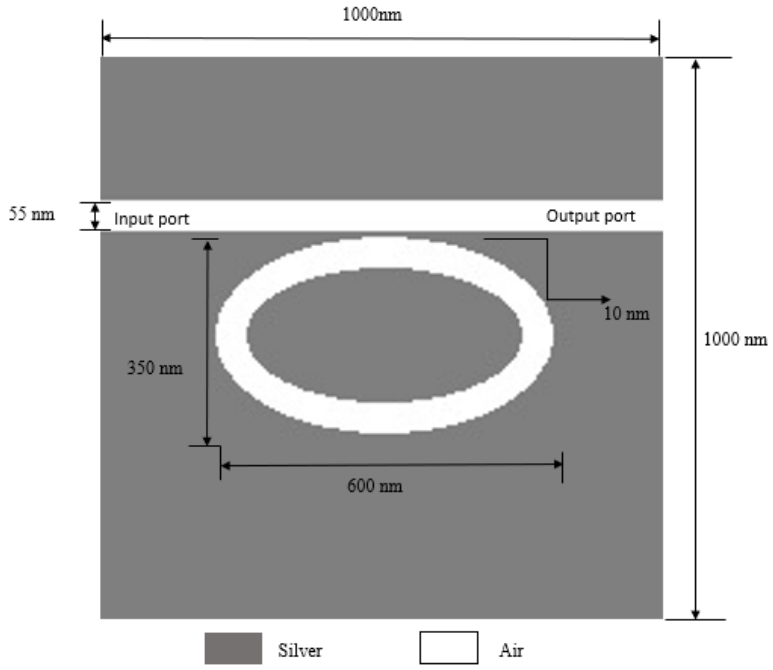

Fig. 7.13: Third elliptical ring structure

7.2.10 Performance Analysis of the Structure

Three notch frequencies can be observed from the plot. These are at approximately 820nm, 1210nm & 1580nm. The notch frequency of 1580nm is a perfect notch frequency because it has 0% efficiency & does not let an energy to pass. The band pass region has shifted to 1580nm-2300nm. The efficiency here is same as the previous two structures. So, the efficiency has not changed considerably for any of the structures. Only the band pass region & notch frequencies have changed. The modes at high transmittance are shown below. The modes are taken at the five peaks which are approximately at 780nm, 1150nm,1450 & 2130nm. These are all odd higher modes.

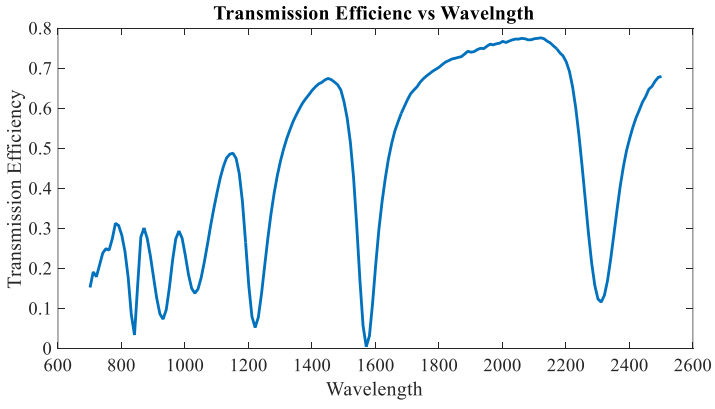

Fig. 7.14: Transmission Efficiency vs Wavelength curve for the third elliptical ring structure

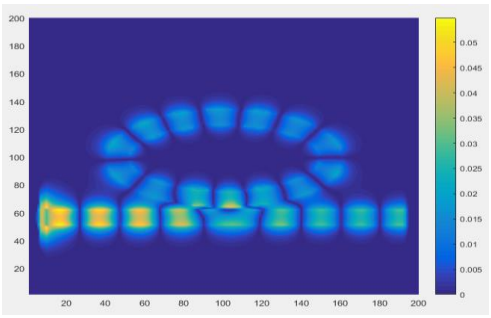

(a)

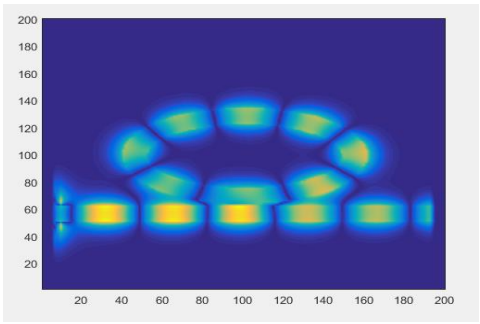

(b)

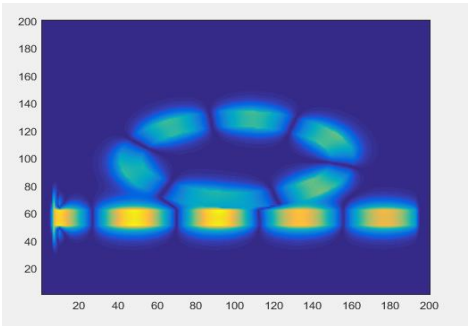

(c)

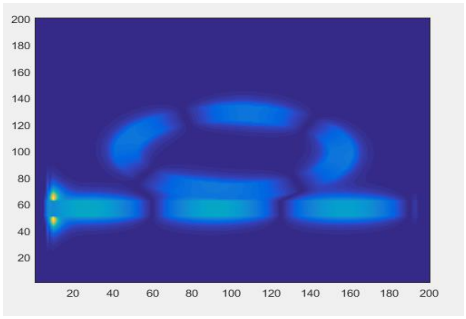

(d)

Fig. 7.15: Mode 13,7, 5 and 3 at wavelengths a) 780nm, b) 1150nm, c) 1450nm and d) 2130 respectively

7.2.11 Rectangular Ring Structures

The geometric shape of the optical ring was again changed to a rectangle. The length of the rectangular ring is 500nm & width of the ring is 300nm. Like previous structures it is also composed 1000nm x 1000nm silver substrate. The input & output ports are also shown in the figure. After developing the structure similar simulation s were made. The transmission efficiency was found out.

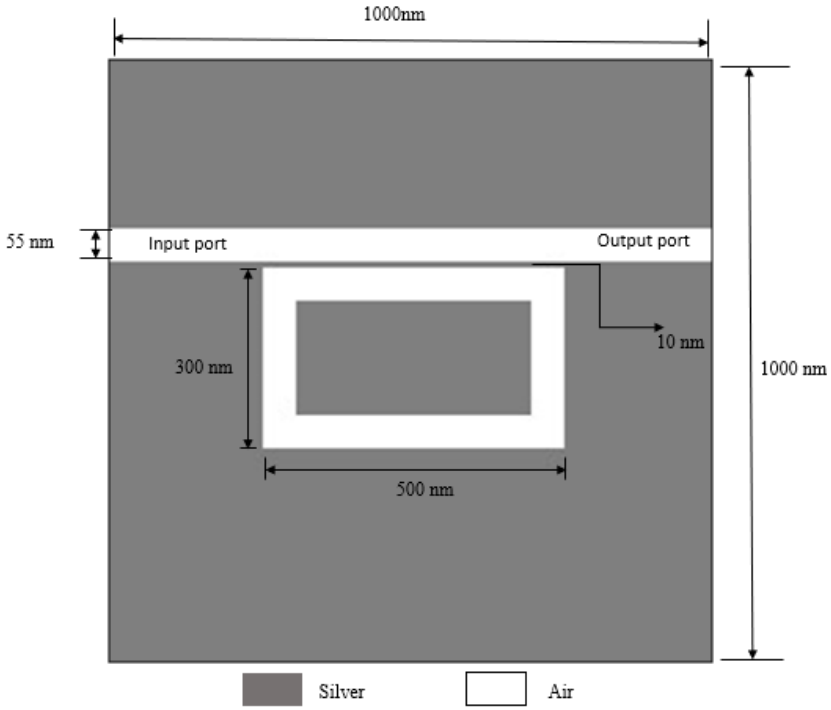

Fig. 7.16: First rectangular ring structure

7.2.12 Performance Analysis of Structure

Two notch frequencies can be observed from the graph approximately at 820nm & 1380nm. The bandpass region is from 1500nm-2350nm. The efficiency of this region is 65%. The efficiency is lower than curved rectangular ring & elliptical ring structure. The modes at high transmittance are again shown below. The modes are taken at the four peaks which are approximately at 1000nm, 1210nm, 1460nm & 2070nm.

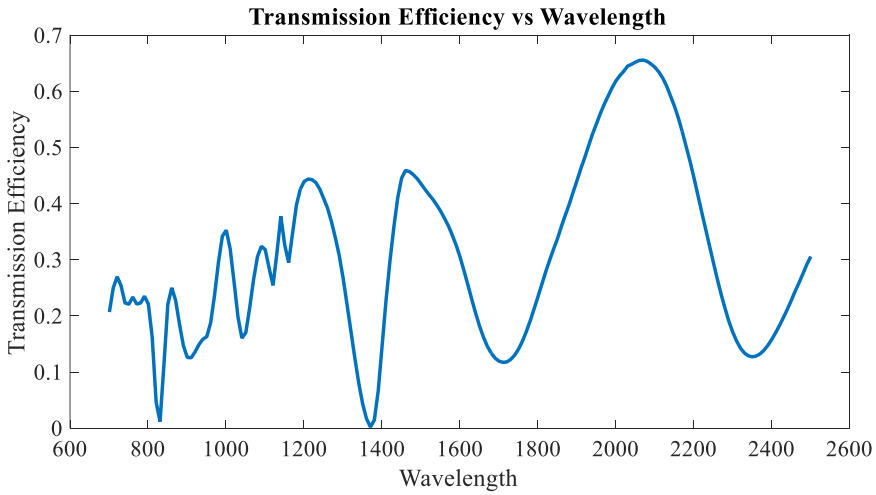

Fig. 7.17: Transmission Efficiency vs Wavelength curve for the first rectangular ring structure

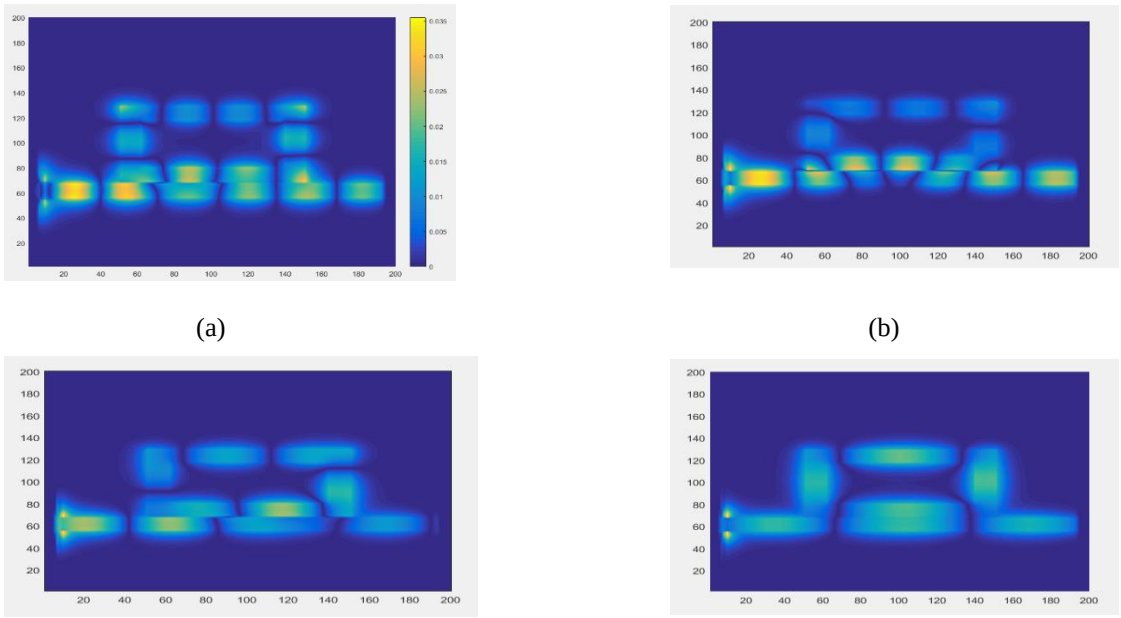

(a) (b)

(c) (d)

Fig. 7.18: Mode 9,7, 5 and 3 at wavelengths a) 1000nm, b) 1210nm, c) 1460nm and d) 2070 respectively

7.2.13 Second Rectangular Ring Structure

The structure parameters were slightly changed from the previous. Only the length of rectangular ring was varied. The length was made 600nm. All the other parameters were kept exactly the same as before. After simulating the structure, we got our desired transmission efficiency vs wavelength curve which is shown below.

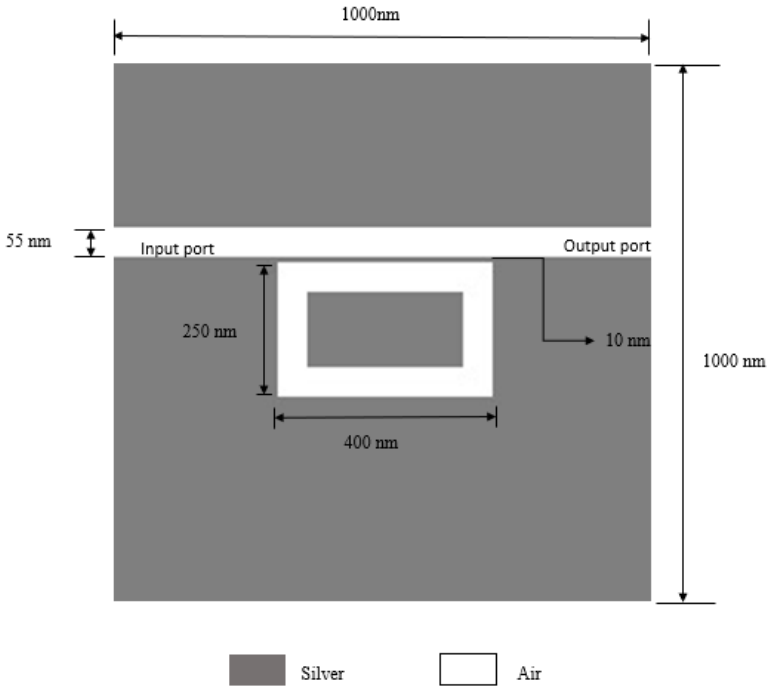

Fig. 7.19: Second rectangular ring structure

7.2.14 Performance Analysis of the Structure

No notch frequencies were obtained from the simulation. The efficiency also became lesser than the previous structures. The band pass region is between 1400nm-1600nm. The FSR observed here is also aperiodic because it is not a circular ring. The parameter changes of the rectangular ring significantly change its output characteristics. The modes are taken at the three peaks which are approximately at 1050nm, 1240nm & 1630nm. These are all odd higher modes.

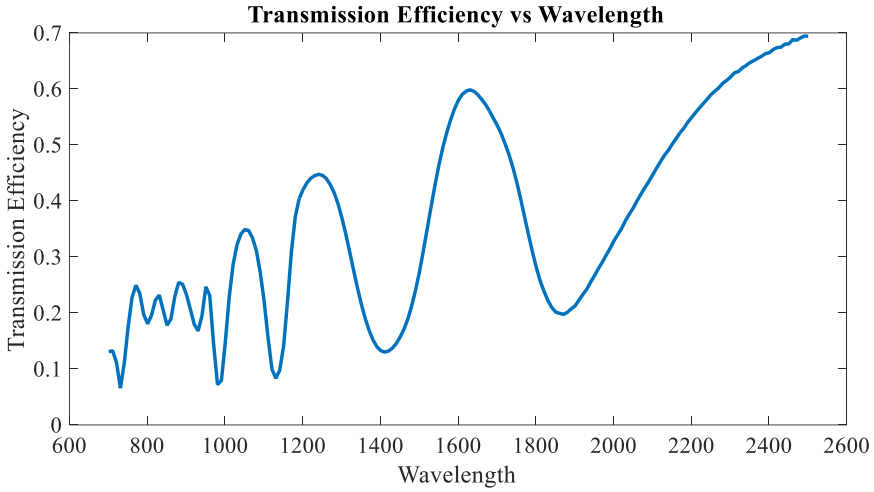

Fig. 7.20: Transmission Efficiency vs Wavelength curve for the second rectangular ring structure

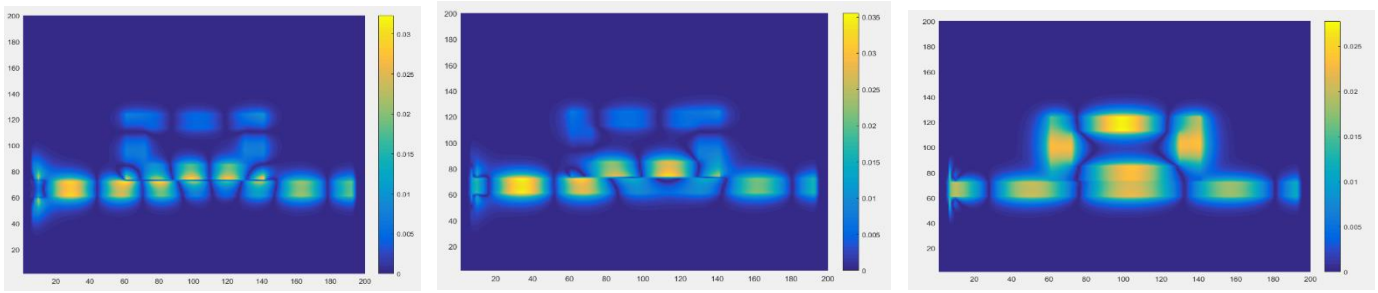

(a) (b) (c)

Fig. 7.21: Mode 7, 5 and 3 at wavelengths a) 1050nm, b) 1240nm and c) 1630nm and respectively

Chapter 8

Future work and conclusion

8.1 Future work

- The proposed designs of the of the high frequency filter has very satisfactory transmission efficiency (about 80-90%) with a very definite cut off wavelength. Since simulation is done by 2D simulator in MATLAB® only, we will simulate these proposed designs by CST Microwave Studio software which will give a better creditability to go for fabrication which is of course still not available Bangladesh.
- We plan to modify the band pass filter structure to find a better performing design which would give a better band pass region.
- We plan to design a low pass wavelength filter in future.
- We plan to develop designs various devices which uses these filters.
- Different devices like logic gates NAND,NOR etc. are also in the queue of our future design plan.

8.2 Paper submission:

A paper written on '**Designing of a Plasmonic High Pass Wavelength Filter With Apodized Grating Waveguide**' is submitted at the 2nd International Conference on Electrical & Electronic Engineering (ICEEE 2017) scheduled to be held on 27-29 December,2017 at Rajshahi University of Engineering and Technology (RUET).

8.3 Conclusion

Plasmonic devices are becoming popular in recent years since it is advantageous over electronics devices. A brief discussion is made in previous chapter about the history of using plasmonic devices and advantages of it.

A nanoplasmonic high pass wavelength or low frequency filter is proposed with inward and outward grating profile apodized by super Gaussian function and also a

band filter is designed by various structure using ring resonator principals. In case of both the filters the cut-off wavelength is varied by varying the structure parameter.

For high pass wavelength filter the grating period and maximum grating width is varied and determined that the grating period doesn't affect cut-off wavelength significantly, but variation of grating width changes cut-off wavelength significantly The variation of cut-off wavelength is directly proportional to the changes in the maximum grating width, i.e cut wavelength increases with the increase of maximum grating width and vice-versa.

Among the nanoplasmonic band pas filter designs, few designs really are useful to fabricate into devices. But some modifications are needed to use the proposed designs directly into fabrication.

References

[1] D. K. Gramotnev and S. I. Bozhevolnyi, "Plasmonics beyond the diffraction limit," *Nature photonics,* vol. 4, pp. 83-91, 2010.

[2] W. L. Barnes, A. Dereux, and T. W. Ebbesen, "Surface plasmon subwavelength optics," *Nature,* vol. 424, pp. 824-830, 2003.

[3] J. Dionne, L. Sweatlock, H. Atwater, and A. Polman, "Plasmon slot waveguides: Towards chip-scale propagation with subwavelength-scale localization," *Physical Review B,* vol. 73, p. 035407, 2006.

[4] M. Z. Alam, J. S. Aitchison, and M. Mojahedi, "A marriage of convenience: Hybridization of surface plasmon and dielectric waveguide modes," *Laser & Photonics Reviews,* vol. 8, pp. 394-408, 2014.

[5] A. J. Haes and R. P. Van Duyne, "A nanoscale optical biosensor: sensitivity and selectivity of an approach based on the localized surface plasmon resonance spectroscopy of triangular silver nanoparticles," *Journal of the American Chemical Society,* vol. 124, pp. 10596-10604, 2002.

[6] C.-W. Lin, J.-H. Lee, N.-F. Chiu, S.-Y. Lee, K.-C. Liu, F.-Y. Tsai, *et al.*, "Hybrid nano plasmonics for integrated biosensor," in *Communications and Photonics Conference and Exhibition (ACP), 2009 Asia*, 2009, pp. 1-6.

[7] S. A. Maier, *Plasmonics: fundamentals and applications*: Springer Science & Business Media, 2007.

[8] R. Djabery, S. Nikmehr, and S. Hosseinzadeh, "Grating effects on sidelobe suppression in MIM plasmonic filters," *Progress In Electromagnetics Research,* vol. 135, pp. 271-280, 2013.

[9] S. A. Maier, "Plasmonics: Metal nanostructures for subwavelength photonic devices," *IEEE Journal of selected topics in quantum electronics,* vol. 12, pp. 1214-1220, 2006.

[10] S. A. Maier, "Plasmonics: The promise of highly integrated optical devices," *IEEE Journal of selected topics in Quantum Electronics,* vol. 12, pp. 1671-1677, 2006.

[11] J. H. Zhu, Q. J. Wang, P. Shum, and X. G. Huang, "A nanoplasmonic high-pass wavelength filter based on a metal-insulator-metal circuitous waveguide," *IEEE Transactions on Nanotechnology,* vol. 10, pp. 1357-1361, 2011.

[12] Y. Chang and C.-H. Chen, "Broadband plasmonic bandstop filters with a single rectangular ring resonator," *IEEE Photonics Technology Letters,* vol. 26, pp. 1960-1963, 2014.

[13] M. Yarahmadi, M. K. Moravvej-Farshi, and L. Yousefi, "Subwavelength graphene-based plasmonic THz switches and logic gates," *IEEE Transactions on Terahertz Science and Technology,* vol. 5, pp. 725-731, 2015.

[14] S. M. Ebadi, S. S. Sajjadi, M. S. Bayati, and S. B. Ram, "A novel plasmonic high pass wavelength filter based on triangular arrays in a MIM waveguide," in *Photonics North*, 2015, pp. 1-1.

[15] A. Hosseini, H. Nejati, and Y. Massoud, "Design of a maximally flat optical low pass filter using plasmonic nanostrip waveguides," *Optics Express,* vol. 15, pp. 15280-15286, 2007.
[16] A. Rahimzadegan, N. Granpayeh, and S. P. Hosseini, "Improved plasmonic filter, ultra-compact demultiplexer, and splitter," *Journal of the Optical Society of Korea,* vol. 18, pp. 261-273, 2014.
[17] M. Ali, K. Lim, A. Becir, M. Lai, and H. Ahmad, "Optical Gaussian notch filter based on periodic microbent fiber Bragg grating," *IEEE Photonics Journal,* vol. 6, pp. 1-8, 2014.
[18] M. Burla, H. P. Bazargani, J. St-Yves, W. Shi, L. Chrostowski, and J. Azaña, "Frequency agile microwave photonics notch filter based on a waveguide Bragg grating on silicon," in *Microwave Photonics (MWP) and the 2014 9th Asia-Pacific Microwave Photonics Conference (APMP), 2014 International Topical Meeting on*, 2014, pp. 392-394.
[19] M. Janipour, M. A. Karami, R. Sofiani, and F. H. Kashani, "A novel adjustable plasmonic filter realization by split mode ring resonators," *Journal of Electromagnetic Analysis and Applications,* vol. 5, p. 405, 2013.
[20] P. Sharma and D. Kumar, "Hybrid metal insulator metal plasmonic waveguide and ring resonator," in *OptoElectronics and Communications Conference (OECC) held jointly with 2016 International Conference on Photonics in Switching (PS), 2016 21st*, 2016, pp. 1-3.
[21] J. Heber, "Plasmonics: Surfing the wave," *Nature News,* vol. 461, pp. 720-722, 2009.
[22] P. B. Johnson and R.-W. Christy, "Optical constants of the noble metals," *Physical review B,* vol. 6, p. 4370, 1972.
[23] E. Jin and X. Xu, "Plasmonic effects in near-field optical transmission enhancement through a single bowtie-shaped aperture," *Applied Physics B: Lasers and Optics,* vol. 84, pp. 3-9, 2006.
[24] J. T. Krug, E. J. Sánchez, and X. S. Xie, "Design of near-field optical probes with optimal field enhancement by finite difference time domain electromagnetic simulation," *The Journal of chemical physics,* vol. 116, pp. 10895-10901, 2002.
[25] A. D. Rakić, A. B. Djurišić, J. M. Elazar, and M. L. Majewski, "Optical properties of metallic films for vertical-cavity optoelectronic devices," *Applied optics,* vol. 37, pp. 5271-5283, 1998.
[26] M. A. Ordal, R. J. Bell, R. W. Alexander, L. L. Long, and M. R. Querry, "Optical properties of fourteen metals in the infrared and far infrared: Al, Co, Cu, Au, Fe, Pb, Mo, Ni, Pd, Pt, Ag, Ti, V, and W," *Applied optics,* vol. 24, pp. 4493-4499, 1985.
[27] G. Veronis and S. Fan, "Bends and splitters in metal-dielectric-metal subwavelength plasmonic waveguides," *Applied physics letters,* vol. 87, p. 131102, 2005.
[28] H. Gao, H. Shi, C. Wang, C. Du, X. Luo, Q. Deng, *et al.*, "Surface plasmon polariton propagation and combination in Y-shaped metallic channels," *Optics express,* vol. 13, pp. 10795-10800, 2005.
[29] B. Wang and G. P. Wang, "Surface plasmon polariton propagation in nanoscale metal gap waveguides," *Optics letters,* vol. 29, pp. 1992-1994, 2004.
[30] G. Veronis and S. Fan, "Theoretical investigation of compact couplers between dielectric slab waveguides and two-dimensional metal-dielectric-metal plasmonic waveguides," *Optics Express,* vol. 15, pp. 1211-1221, 2007.
[31] P. Ginzburg and M. Orenstein, "Plasmonic transmission lines: from micro to nano scale with λ/4 impedance matching," *Optics express,* vol. 15, pp. 6762-6767, 2007.

[32] D. Pile and D. K. Gramotnev, "Adiabatic and nonadiabatic nanofocusing of plasmons by tapered gap plasmon waveguides," *Applied Physics Letters*, vol. 89, p. 041111, 2006.
[33] R. Wahsheh, Z. Lu, and M. Abushagur, "Nanoplasmonic air-slot coupler: design and fabrication," in *Frontiers in optics*, 2012, p. FTh4A. 6.
[34] Y. Wang, "Surface-plasmon-wave-coupled tunable filter," ed: Google Patents, 1999.
[35] S. Khan and S. Fathpour, "Demonstration of tunable optical delay lines based on apodized grating waveguides," *Optics express*, vol. 21, pp. 19538-19543, 2013.
[36] S. Khan and S. Fathpour, "Complementary apodized grating waveguides for tunable optical delay lines," *Optics express*, vol. 20, pp. 19859-19867, 2012.
[37] S. Khan, M. A. Baghban, and S. Fathpour, "Electronically tunable silicon photonic delay lines," *Optics Express*, vol. 19, pp. 11780-11785, 2011.
[38] E. Verhagen, "Subwavelength light confinement with surface plasmon polaritons," Utrecht University, 2009.
[39] A. Archambault, T. V. Teperik, F. Marquier, and J.-J. Greffet, "Surface plasmon Fourier optics," *Physical Review B*, vol. 79, p. 195414, 2009.
[40] R. Luebbers, F. P. Hunsberger, K. S. Kunz, R. B. Standler, and M. Schneider, "A frequency-dependent finite-difference time-domain formulation for dispersive materials," *IEEE Transactions on Electromagnetic Compatibility*, vol. 32, pp. 222-227, 1990.
[41] D. F. Kelley and R. J. Luebbers, "Piecewise linear recursive convolution for dispersive media using FDTD," *IEEE Transactions on Antennas and Propagation*, vol. 44, pp. 792-797, 1996.
[42] R. J. Luebbers, F. Hunsberger, and K. S. Kunz, "A frequency-dependent finite-difference time-domain formulation for transient propagation in plasma," *IEEE Transactions on Antennas and Propagation*, vol. 39, pp. 29-34, 1991.
[43] R. J. Luebbers and F. Hunsberger, "FDTD for Nth-order dispersive media," *IEEE transactions on Antennas and Propagation*, vol. 40, pp. 1297-1301, 1992.
[44] F. Hunsberger, R. Luebbers, and K. Kunz, "Finite-difference time-domain analysis of gyrotropic media. I. Magnetized plasma," *IEEE Transactions on Antennas and Propagation*, vol. 40, pp. 1489-1495, 1992.
[45] A. Akyurtlu and D. H. Werner, "BI-FDTD: A novel finite-difference time-domain formulation for modeling wave propagation in bi-isotropic media," *IEEE Transactions on Antennas and Propagation*, vol. 52, pp. 416-425, 2004.
[46] A. Grande, I. Barba, A. C. Cabeceira, J. Represa, P. P. So, and W. J. Hoefer, "FDTD modeling of transient microwave signals in dispersive and lossy bi-isotropic media," *IEEE transactions on microwave theory and techniques*, vol. 52, pp. 773-784, 2004.
[47] A. Akyurtlu and D. H. Werner, "A novel dispersive FDTD formulation for modeling transient propagation in chiral metamaterials," *IEEE Transactions on Antennas and Propagation*, vol. 52, pp. 2267-2276, 2004.